Different Heat Treatment parameters investigation on microstructure, mechanical and wear properties of Hadfield Steel

Vishwajit Vishnu Kolekar
Rahul Milind Kulkarni

2021

CODEN:LUTMDN/(TMMV-5325)/1-88/2021

LUND UNIVERSITY

LTH

FACULTY OF ENGINEERING

MASTER THESIS
DIVISION OF PRODUCTION AND MATERIALS ENGINEERING
LUND UNIVERSITY

LTH supervisor: Latifa Melk. Dr.
Examiner: Jan-Eric Ståhl, Professor

Authors: Vishwajit Vishnu Kolekar and Rahul Milind Kulkarni
Lund, Sweden 2021

Avdelningen för Industriell Produktion
Lunds Tekniska Högskola
Lunds universitet
Box 118
221 00 Lund
Sverige

Division of Production and Materials Engineering
LTH, School of Engineering
Lund University
Box 118
SE-221 00 Lund
Sweden

Printed in Sweden
Media-Tryck
Lund University

“*The finest steel has to go through the hottest fire.*”

-Richard M. Nixon, 1973

Acknowledgment

We would like to express our deep sense of gratitude towards the company for providing us with the opportunity to carry out this thesis. This thesis would not have been possible without the support, patience, and encouragement of our supervisor Dr. Latifa Melk, not to mention her advice, dynamism, inquisitiveness, and unsurpassed knowledge in Materials Engineering have constantly motivated us. Furthermore, we would like to thank Jörgen Petersson, Foundry Specialist, for his valuable comprehensions and the rest of the company for assisting us directly or indirectly.

Special thanks to Axel Bjerke, Ph.D. Student for his insights and valuable time for helping us in the Lab. Additionally, we would like to thank Dr. Christina Windmark for her advice, and her support has been indispensable.

We would also like to thank our examiner, Jan-Eric Ståhl, and the Division of Production and Materials Engineering, Department of Mechanical engineering, Faculty of Engineering, Lund University, who got us the opportunity to write our master thesis at such a large and respected Swedish corporation and helped us by providing all the necessary support and knowledge to complement this thesis.

We are incredibly grateful to our parents for their unequivocal support, love, care, prayers, and scarifies for educating and preparing us for our future. Nothing would have been possible without them.

It would have been merely impossible to ensure this thesis in its best shape without help and support from our friends and the kind people around us.

Finally, lord almighty is worthy of all the acknowledgments; we will keep trusting in you for our future.

Lund 2021-06-09

Vishwajit Vishnu Kolekar & Rahul Milind Kulkarni

Abstract

Hadfield Steels make up a significant group of steels that can perform with their higher strength, excellent wear resistance, and good formability. To achieve this distinctive behavior along with the alloy compositions, heat treatment is also a vital factor. Alloy carbides can be controlled with various heat treatment techniques, as they directly affect the loss in strength, which eventually leads to making the material more brittle. The changing times require all the materials to be more efficient from all the perspectives one could ever imagine. The steel industry must continue to look into the introduction of unique heat treatment techniques. The current study examines the microstructure using Optical Microscope (Alicona), Scanning electron microscopy (SEM), Energy dispersive spectroscopy (EDS) followed by mechanical characterization of three different Hadfield Steel Grades (X, Y, and Z) after implementing different heat treatment cycles and an aqueous quenching medium in this frame of reference. To complement this experimental work, an extensive literature review has been carried out to foresee the outcomes. This study reveals that Steels X and Y behave identically to the implemented heat treatment cycles as they have similar microstructures, Z has more admirable grain boundaries. All the grades (X, Y, and Z) show their tendency towards the optimal hardness values accordingly to the Heat Treatment cycle. Categorized based on the heat-treatment used, the microstructures were mostly austenite matrix both with and without carbides at either the grain boundaries and in the austenitic grains in all scenarios. To sum up, this is a vast area to explore. All the small details concerning the heating and quenching play a crucial role in developing the heat treatment cycle and so the Hadfield steel.

Keywords: Hadfield Steel, Heat Treatment, Microstructural evolution, Carbides, Austenitization temperature

Table of Content

List of Figures

List of Tables

List of Abbreviations

Abbreviations	Meaning
ASTM	American Society for Testing and Materials
BCC	Body-Centered cubic
BCT	Body-Centered tetragonal
EDM	Electric Discharge Machine
EDS	Energy-dispersive spectroscopy
FCC	Face- Centered Cubic
HT	Heat Treatment
OM	Optical Microscope
SEM	Scanning Electron Microscope
TTT	Isothermal Transformation Diagram

1. Introduction

1.1. Background

Sir Robert Hadfield discovered Manganese steel/Hadfield steel in the year 1882. This type of steel is also known as Mangalloy. This type of steel is High alloy steel with a Carbon content ranging from 1.1%-1.4%, and the Manganese content ranges from 11%-14%. This type of steel is unusual because it blends good strength and ductility with such a good vulnerability for work-hardening and strong resistance to abrasion. This type of steel is usually classified as ASTM A128, and this steel family was dedicated to the memory of Sir Robert Hadfield. After different trials, Robert Hadfield managed to show that, combined with high wear resistance, a particular form of austenitic steel could have exceptional durability. Veladimir Lipsin followed his study on the topic of manganese on such steel [1]. Just up to 2.46% of manganese content in the steel had been examined in previous work, so that is where the experiments of Hadfield began. Using a ferromanganese alloy of 80% manganese and 7% carbon, series of steels have been made. An estimated 10:1 ratio of manganese to carbon has been developed due to the use of this alloy. It was observed that the steels were surprisingly brittle in the range of 2.5 - 7.5 % manganese, but the steels were surprisingly tough once the manganese content surpassed 10%. Furthermore, with quenching in cold water after heating to 1000°C, the toughness of the material increased [2].

While some modern materials are presently available which could be used as a substitute for this material, manganese austenitic steels are exceptional in their own rights since they have an optimal method of durability, strength, high resistance to abrasion. Over the last century, it has received significant attention as an engineering material. It is widely used in the fields of earthmoving, mineral extraction, smelting, oil well excavation, railing, dredging, woodworking, and concrete and clay processing [3]. These steels can be used in the automotive industry, recycling industries, and military, among other applications. The typical metals including high chromium iron, hyper-steel, casehardened mild carbon steel, and manganese steel. In practical terms, the high chromium iron suitable for wear-resistant purposes

falls inside the elemental limits bound by the austenitic phase area of the iron, Chromium, carbon phase diagram surface of both the ternary liquidus region [4]. Because the Hadfield Steels have high C and Mn content, their cast structure comprises austenite grain with carbides dispersed in the grain borders. This type of structure is brittle as well as often ineffective [5]. Fast quenching of Hadfield steel after austenitization heat treatment in a salt bath can prevent grain boundary carbides accumulation [6]. Its structure in the form of casting contains carbide phases such as $(Fe,Mn)_3C$, on which a complete austenitic structure can be formed with adequate heat treatment. The austenitic single phased microstructure will be formed after an austenitizing and quenching heat treatment [6]. The specified alloy will achieve the required hardness through heat treatment. The implementation of heat treatment results in the appropriate mechanical properties. As a result, the dissolving temperature must be high enough to dissolve the carbides in austenite. To achieve a supersaturated matrix, rapid quenching of the austenite's single-phase structure is essential [6], and therefore there is the need for our study to come in.

1.2. Objectives of this thesis project

The goal of this thesis is to study and investigate the effects of various heat treatment cycles for the existing Hadfield Manganese steel grades with improved microstructure and mechanical properties. The study will provide insight into current and new heat treatment cycles and a variety of quenching methods to give a better interpretation.

The key emphasis will be to study the microstructural evolution of these steels subjected to various heat treatment cycles. Which is to lower the carbides and improve grain boundaries which will further improve toughness without affecting other properties by mechanical tests and microstructural analysis of Hadfield steel. The literature study can also be used to visualize out every variety of heat treatment methods, which will aid in determining what parameters to focus on to improve the manganese alloys, helping to eliminate the key difference between the theoretical and practical approach. Therefore, this study employs a multidimensional approach that includes experimental and analytical elements to determine logical and quantitative

growth alternatives and then improve understanding through estimating the consequences of improvements in the manufacturing of the Hadfield steel, especially from the point of heat treatment.

1.3. Layout of the thesis project

This thesis report is divided into six different chapters; the first introduction chapter explains the background and objective of the thesis, followed by a literature review. The experimental procedures are then carried out, which will be followed by results and discussion. Finally, some opinions about the significant scope and objectives are derived.

2. Literature Review

This chapter gives us some fundamental theory descriptions regarding compositions, phase diagrams, heat treatment, quenching, and carbides. The description of these topics would benefit in establishing the context and help clarifying some of the concepts used throughout this thesis.

2.1. Hadfield Steel

British Patent Number 200 was issued to Sir Robert Hadfield in 1883. Later, In the United States, Patent No. 303150 and 303151 were registered in 1884 [7]. Before using electric furnaces, from the year 1919, by infusing molten carbon steel with separately melted ferromanganese, most manganese steels were produced in a cupola furnace, low phosphorus pig iron and steel scrap were melted, then blown in a Bessemer type converter, and ferromanganese melted in crucibles in special furnaces, blended mostly with blown steel in a ladle [7]. For many of the manganese steels made even to this day, obtaining the Hadfield steel is still the fundamental goal. Since the invention of this steel alloy, chemistry has not evolved significantly. Most manufacturers sell identical products even without several balanced approaches, with specific differences in the carbon level; however, these alloy steels are approximately 12% manganese. These steels do have the potential to harden both in action and by forced methods in depth. Work hardening, as from hammer strikes, is usually caused by impact. Light blows cause shallow deformation with only superficial hardening, even though they are high velocity, even if the resulting fracture toughness is typically high. Hadfield manganese steel is unmatched in its ability to harden, outpacing even metal-stable austenitic stainless steel [8].

Coming to the hardness characteristics, we usually see about 200 HB in the annealed solution and water agitated state. This material can be hardened to approximately 500 HB by pressure [9]. The impact loading must be high to achieve this high hardness level, whereas the material abrasion from gouging abrasion is minimal. Also, Carbides are crucial in this case to change the properties of this material. So, a rational solution seemed to lie in the development of properly distributed hard carbides in the austenitic matrix of

the steel to increase the wear resistance of austenitic manganese steels. While, at the very same period, adversely harming its durability [10].

2.2. Chemical Compositions

In Hadfield steel, the most general composition for carbon is 1.2%, and manganese ranges from 10-14%. The Most common ASTM Specifications are listed in the following table.

Table 1: *Standard Grades ASTM A128 Composition [11]*

ASTM Grade	Composition (%)						
	C	**Mn**	**Cr**	**Mo**	**Ni**	**Si**	**P**
A	1.05-1.35	11.0	-	-	-	1.0	0.7
B-1	0.9-1.05	11.5-14.0	-	-	-	1.0	0.7
B-2	1.05-1.2	11.5-14.0	-	-	-	1.0	0.7
B-3	1.12-1.28	11.5-14.0	-	-	-	1.0	0.7
B-4	1.2-1.35	11.5-14.0	-	-	-	1.0	0.7
C	1.05-1.35	11.5-14.0	1.5-2.0	-	-	1.0	0.7
D	0.7-1.3	11.5-14.0	-	-	3.0-4.0	1.0	0.7
E-1	0.7-1.3	11.5-14.0	-	0.9-1.2	-	1.0	0.7
E-2	1.05-1.45	11.5-14.0	-	1.8-2.1	-	1.0	0.7
F	1.05-1.35	6.0-8.0	-	0.9-1.2	-	1.0	0.7

The mechanical and physical properties of austenitic manganese steels differ according to the content of carbon and manganese. Because as a minimum percentage of the composition spectrum is correlated with weaker tensile properties, there has been a probability of function near the midpoint carbon scale. With 12-13 % Mn and the higher limit has no added value [12].

2.2.1. Carbon

Carbon, along with manganese, is indeed one of the two most critical elements in Hadfield manganese steel. A supersaturated solution of Carbon is Hadfield manganese steel. Carbon and manganese have an average ratio of 1:10 to the standard grade of Hadfield manganese steel. Therefore, 12% of manganese and 1.2% of carbon are usually present in this steel. Carbon does have a minor but significant impact on yield strength; decreasing the quantity of carbon induces yield strength to reduce. Factors and grain size

outweigh the effects of carbon content on specific tensile properties, but there is a tentative suggestion of about 1.15 percent optimal carbon composition. By forming embrittling-type carbide boxes along grain boundaries or even as plates along crystallographic planes, higher carbon content than 1.25 percent generally tends to embrittle steel [7]. The carbon content influences Hadfield manganese steel's yield strength. Carbon concentrations below 1% cause the intensity of the yielding to drop. Around 1 % and 1.2 % were considered to be the ideal carbon content. Yield intensity is unaffected, above 1.2 % carbon content [12]. Specific alloying components such as Chromium enhance the strength of the yield but minimize ductility. Increased concentrations of carbon may indeed create issues throughout the heat treatment process or in the foundry. Low carbon content effectively prevents the embrittling impact of carbide precipitation through cooling below the solubility point [12].

2.2.1.1. Effect of carbon content on hardenability

The carbon content highly determines hardness. To improve both hardness, carbon can be used. The number and form of alloying elements present significantly enhance this Effect. The inclusion of carbon up to the eutectoid content increases hardenability as the rise in carbon content is related to increased hardenability [13]. The formation of pearlite and proeutectoid constituents become more complex as the carbon content of the steel increases. The declaration also holds for hypereutectoid steels, providing that each steel is fully converted to austenite before its hardenability is measured [14].

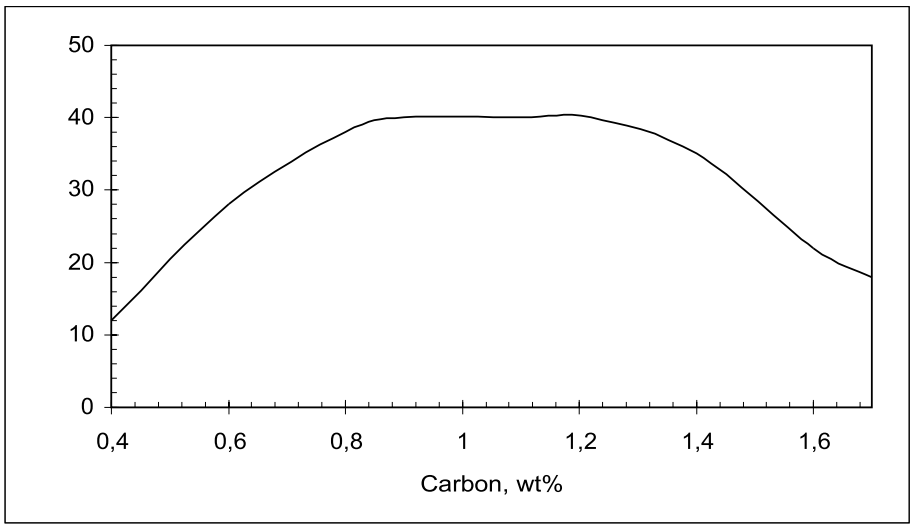

Figure 1 : *Effect of carbon content on ductility of the 12-14Mn Hadfield steels [9]*

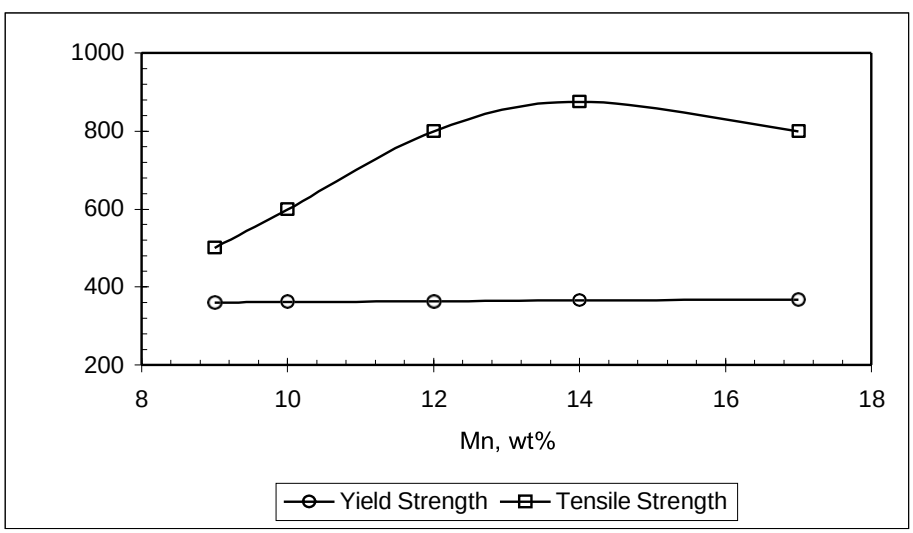

Figure 2 : *Effect of Mn content on tensile and yield strength of Hadfield steels [9]*

2.2.2. Manganese

The family of Hadfield manganese steels is made possible by manganese being an austenite stabilizer. It lowers the phase transition of the austenite to ferrite and thus helps to preserve a completely austenitic structure at room temperature. With 13 % manganese and 1.1 % carbon, Hadfield manganese steel have a starting martensite temperature under 200°C [2]. Also, the lower bound for the amount of manganese in plain austenitic manganese steel is almost 10%. Manganese adds to the activity of a critical austenite firm reliance to prolong transformation instead of removing it [2]. Manganese has practically no effect on yield strength within the range of 10-14 %. However, tensile strength and ductility benefit from it. It is possible to distinguish the correlation between 10% and 13% manganese, but it requires careful monitoring of other parameters to say clearly. Studies have also shown that the tensile properties decrease quickly, sometimes to half of their usual level at around 8% Mn, below 10 percent Mn. 11% Mn is ideal as a minimum for critical requirements, even if the increase over 10% is minor [2]. The limit is somewhat subjective and is likely to rely mainly on the cost of the alloy than on the machining performance, as up to at least 20% Mn can be produced with appropriate properties. The ratio of Mn-C ratio is 10:1 [2].

Because of the better carbide dispersion and partly because of the less stable austenite in the lower manganese steels, the lower manganese content will provide better wear resistance. The decreased manganese steels with their lower strength should be functional in several applications in order to acquire enhanced wear resistance [2].

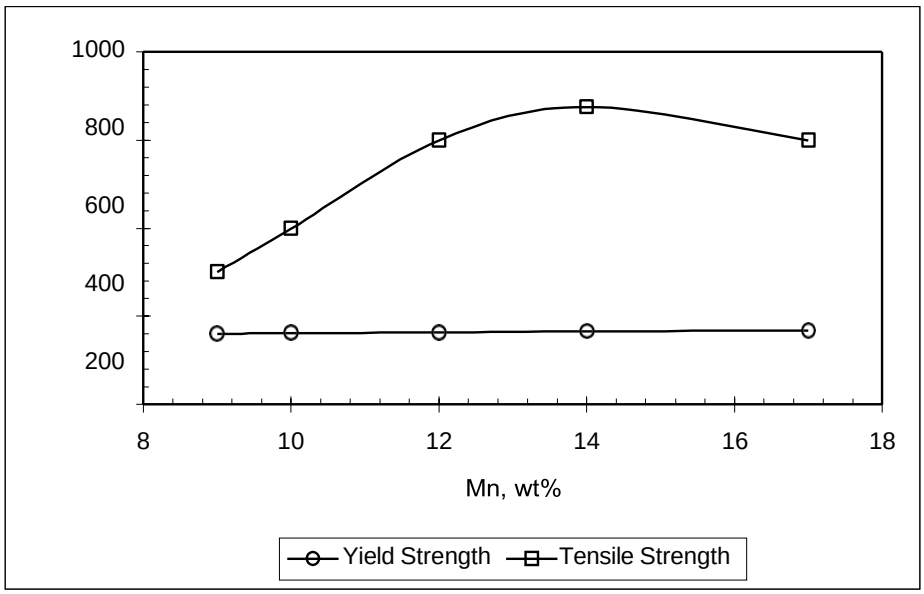

Figure 3 : *Effect of Mn content on tensile and yield strength of Hadfield steels [9]*

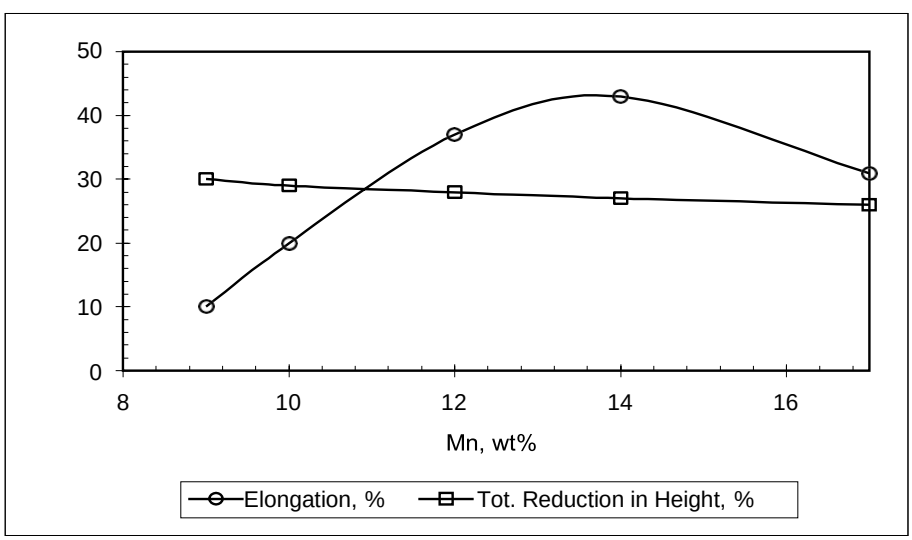

Figure 4 : *Effect of Mn contenton elongation and total reduction in height of Hadfield steels [9]*

2.2.3. Chromium, Nickel, and Molybdenum

Intriguingly, Chromium effect is close to that of increasing the carbon level in heavier sections; the outcome is a reduction in ductility related to a rise in carbide volume fraction in the microstructure. According to the research, adding Cr to high manganese steel increases hardness and wear resistance while decreasing toughness [15]. For welding electrodes, nickel and molybdenum additions are favoured. Molybdenum contributions, usually 0.5%-2%, are made to enhance the strength and durability of castings to cracking in the as-cast state and to increase the yield strength of large section castings in the handled and quenched state of the solution [2].These events arise when, in Manganese steel, Molybdenum is distributed partly in the austenite solution and partially in the primary carbides produced during steel solidification. Even when the austenite is exposed to temperatures above 275 °C during welding or in operation, the Molybdenum in solution essentially suppresses the formation of both fragile carbide precipitates and pearlite [7].

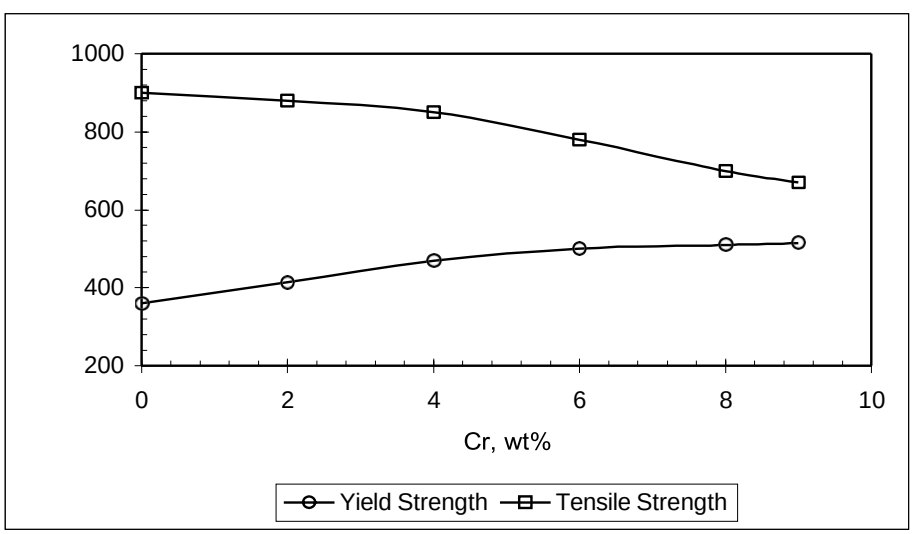

Figure 5 : *Effect of Cr addition on yield and tensile strength of 12-14 Mn Hadfield steel [9]*

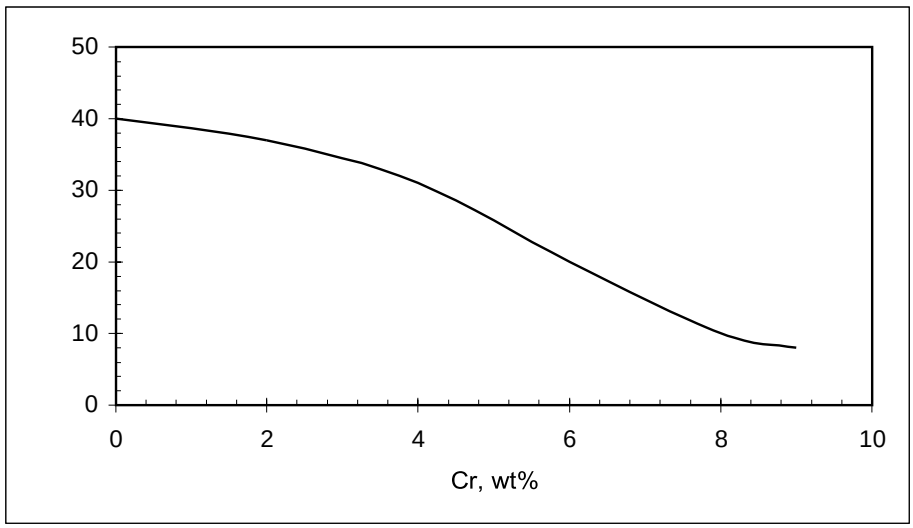

Figure 6 : *Effect of Cr addition on ductility of 12-14 Mn Hadfield steel [9]*

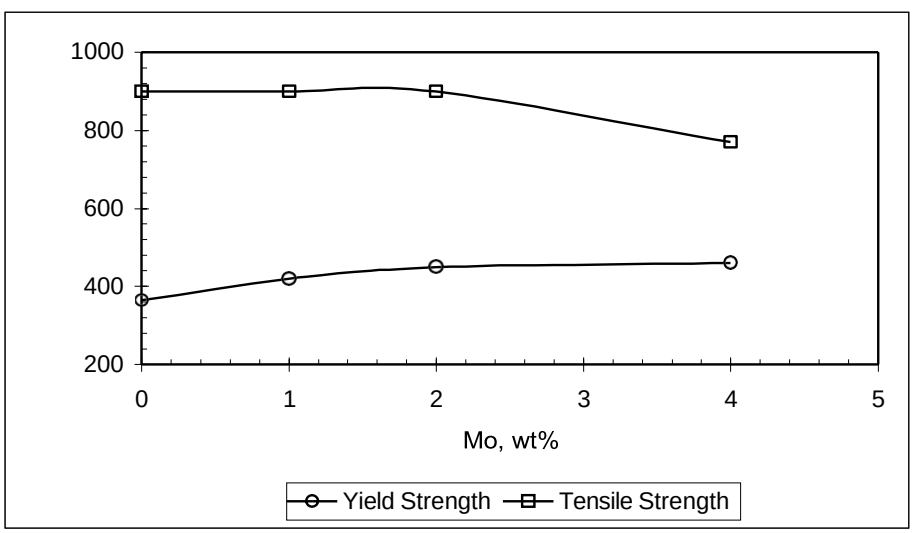

Figure 7 : *Effect of Mo addition on yield and tensile strength of 12-14 Mn Hadfield steel [9]*

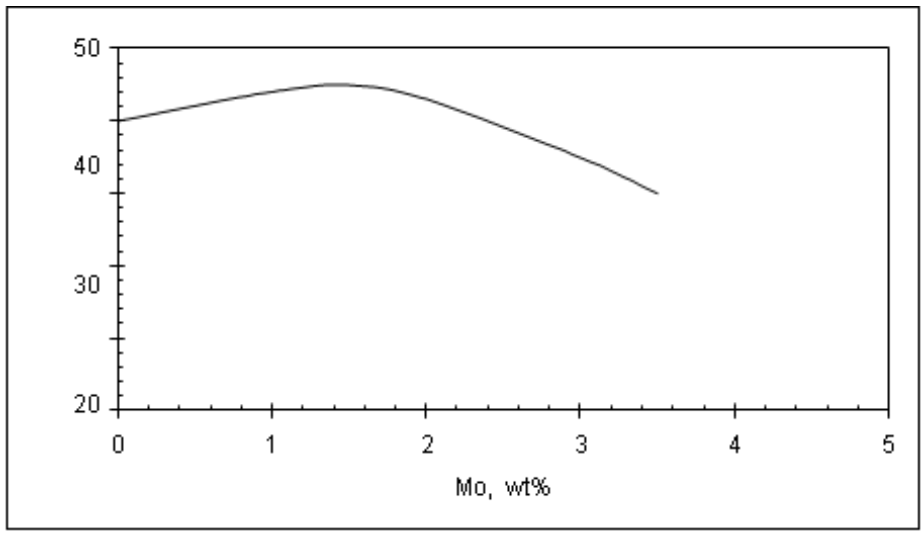

Figure 8: *Effect of Mo addition on the ductility of 12-14 Mn Hadfield steel [9]*

2.3. Phase Diagrams

The term phase is used in metallurgy to relate to a physically homogeneous state of matter. This phase has a particular chemical composition and a different kind of atomic binding and element configuration. Two or more distinct phases may be present simultaneously in an alloy. A graph showing the presence of various stages of a system under equilibrium is called a phase diagram [16]. Usually, this is a set of curves to limited solubility. They are often recognized as balance or constitutional diagrams. Each phase will have its own distinguishable mechanical, electrical, physical, and electrochemical characteristics within an alloy [16]. The phases of an alloy rely on the concentration of the alloy and the heat treatment to which the alloy has been subjected [16]. An alloy's phase changes can be predicted using phase diagrams, which have been subjected to a complex heat-treatment process. For metallurgists, phase diagrams are helpful for the selection of alloys with a particular composition, simulation, and optimization of processes. For the heat treatment process, which generates specific properties, they can also be used for addressing quality control issues. Phase diagrams show which phases in an alloy are thermodynamically stable and could be assumed to be active for a prolonged period when the component is exposed to a specific temperature [16]. The phase diagrams are named as urinary to decenary, depending on several components.

2.3.1. Iron Carbon Phase Diagram

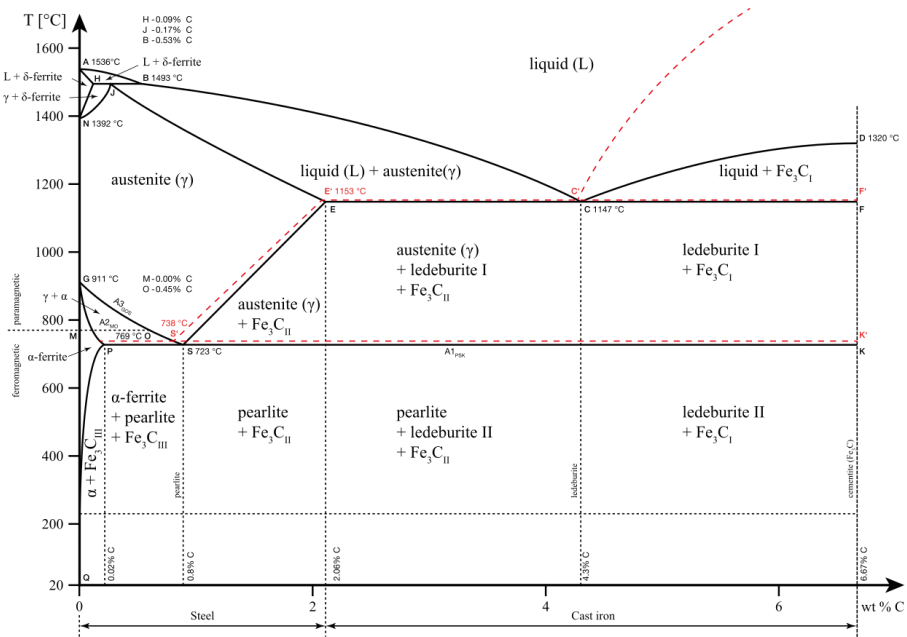

Figure 9 : *Iron Carbon Phase Diagram [17]*

To explain the various phases of steel and cast iron, the iron-carbon phase diagram is most often used (Figure 9). A mixture of iron and carbon are both steel and cast iron. Both alloys often contain a limited quantity of trace elements. In this phase diagram, up to 6.67 weight percent (wt%) of carbon can be studied. The scale of the graph is the temperature on Y-axis and weight on X-axis [18]. While the metal temperature rises or decreases, as the temperature exceeds the value on the boundary, phase transition at these borders [18]. As the temperature is increased, the heating leads to a reshuffling of the structure into some kind of a new phase, so the temperature halts rising before the phase has actually shifted, as the temperature stays stable; this is known as a thermal arrest [18]. The location of such boundaries on the phase diagram is influenced by alloy steel elements such as nickel, manganese, Chromium, and molybdenum. Depending on the element used, the boundaries can change in either direction [19].

2.3.1.1. Characteristics of Phases

- **Ferrite (α):** Ferrite is considered a solid solution of carbon and other alloying elements in a body-centered cubic iron [20]. Also known as α-iron. This is a reliable interstitial solution soluble in alpha iron with a limited quantity of carbon. The mean solubility at 723 ºC is 0.025 %C, and just 0.008 %C dissolves at ambient temperature. It is also the lightest composition that occurs on the graph. [21] It is soft, ductile, and has a hardness of 70-100 BHN and reasonably high conductivity [22]. The carbon-free austenite is converted into ferrite, which is essentially pure iron steel when austenitized steel is cooled below A_h. Usually, the Hardness is 70-100 BHN, and Tensile strength is 245 Mpa, and Yield strength 118 Mpa.

- **Cementite (Fe_3C):** Cementite is the iron and carbon compound chemically recognized as iron carbide with the estimated chemical formula Fe_3C 6.67 %C. It is distinguished by a crystalline structure that is orthorhombic. Usually, this is a low tensile strength (35 Mpa) hard and brittle interstitial compound, but compressive solid strength and high toughness [21]. This is the most rigid structure to appear on the graph. Up to 210 ºC, it is mildly ferromagnetic, and above it is paramagnetic. The melting temperature is 1227 ºC.

- **Pearlite (α+Fe_3C):** Pearlite is a 0.80 %C eutectoid mixture and is formed at 723 ºC on prolonged cooling. This is an excellent plate of ferrite and cementite or lamellar mixture. Pearlite is a precise signature combination [21]. The weight percentage ratio is 8:1. The hardness is BHN 200-300 with a tensile strength of around 825Mpa. A certain quantity of proeutectoid cementite begins to form before the pearlite, as a continuous network at the austenite grain limits, throughout the event of hypereutectoid steels (>0.8% C). It could also have a lamellar pearlite infill [22]. Usually, we can find it in annealed or normalized steels. This structure can be observed [20].

- **Austenite (γ):** This is an interstitial solid solution with a minimal quantity of carbon dissolved in gamma iron and the composition of the FCC crystal [21]. At 1147 ºC, the maximum solubility is 2.1% C. Austenite is soft, ductile, and FCC structure and non-magnetic

[21]. Steels are usually rolled and forged above 1100 ºC, while they are in the austenite state due to their higher ductility and malleability, which would also be attributable to their FCC structure [21]. We find higher toughness, and the Tensile strength is around 1035 Mpa.

- **Ledeburite (γ+Fe_3C):** The eutectic mixture of austenite and cementite is ledeburite. It contains 4.3 percent C and at 1147 ºC is formed [22]. Tiny islands of austenite are scattered in the carbide process within the formation of ledeburite. Unstable at room temperature [21].

- **Ferrite (δ):** This has a BCC structure. It is an interstitial solid solution dissolved in alpha iron with a limited quantity of carbon. The mean solubility at 723 ºC is 0.025 % C, and just 0.008 % C disperses at room temperature [22]. It is the softest composition that occurs on the graph. Ferrite is ferromagnetic at low temperatures. However, with the increase of temperatures with large losses at curial temperatures of 768 ºC or above this temperature, it begins to lose its magnetic properties and becomes paramagnetic. Hardness is 95 VPN, Yield strength is 118 Mpa, and Tensile Strength 245 Mpa [21].

- **Martensite:** The term "martensite" was adopted in the year 1890 to honor Adolf Martens' metallographic investigations, often used to define the quenched steel's hard phase [22] [23] [24]. In steels, martensite transition happens most often upon rapid cooling above on austenitic temperatures, also known as quenching, when the cooling rate is necessary to avoid significant diffusional solid-state transformations, such as ferrite and pearlite [24]. The martensite transition can be explicitly or implicitly completed at room temperature, based on the amount of carbon and alloying elements present in the structure [21]. Hardenability denotes a steel's ability to create martensite after quenching and the threshold cooling rate required for such a martensitic transition [22]. The lattice structure depends on the carbon content of the steel. It varies from a body-centered tetragonal (BCT) to Body-centered cubic (BCC) [22].

2.3.1.2. Critical Temperatures

The temperature ranges are usually represented with various Greek letters. The following mentioned temperatures are generally important in the phase diagram [25]:

723 ºC: Perlite Point, A1 point eutectoid transformation

769 ºC: Ferromagnetic, α iron A2

911 ºC: Non-magnetic, α iron A3

1392 ºC: γ - iron, A4

1536 ºC: Solidification Temperature, δ – iron

2.3.2. Iron Manganese Phase Diagram

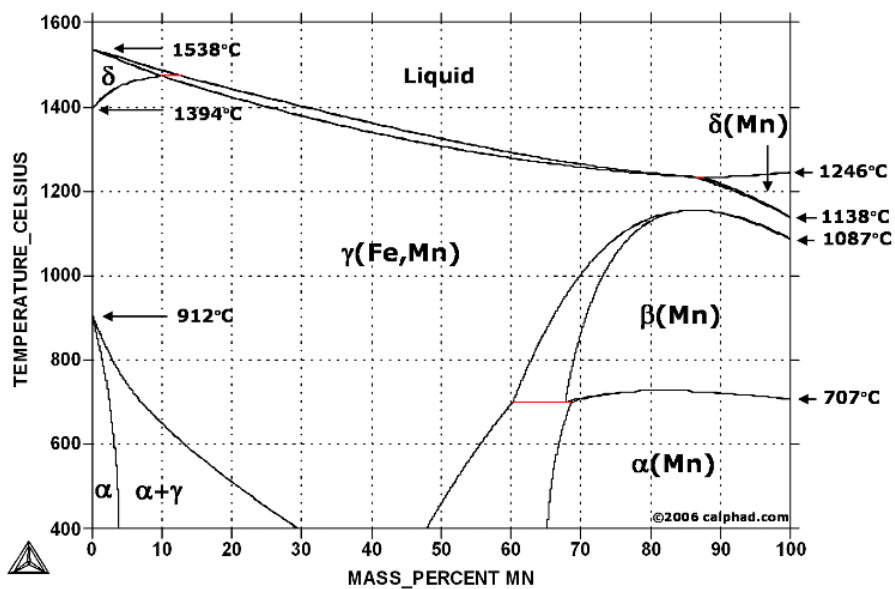

Figure 10 : *Iron-Mn Phase diagram [26]*

In the Figure 10, we can see the Fe-Mn Phase diagram, which shares a lot of information about the phases which can be expected to be in equilibrium for the various percentage of Mn. The A4 (1394 ºC) and A3 (912 ºC)

temperature changes occur at ambient temperature [25]. When an element enters a solid solution in iron, thus forming a binary alloy, each one of these transitions is expected to occur throughout a range of temperature by the phase law. The melting point for Fe is noted at 1538 Mn at 1 atm pressure is recorded around 1538 ºC and Mn is noted at 1246 ºC. This is usually FCC type [27].

2.3.3. TTT Diagram

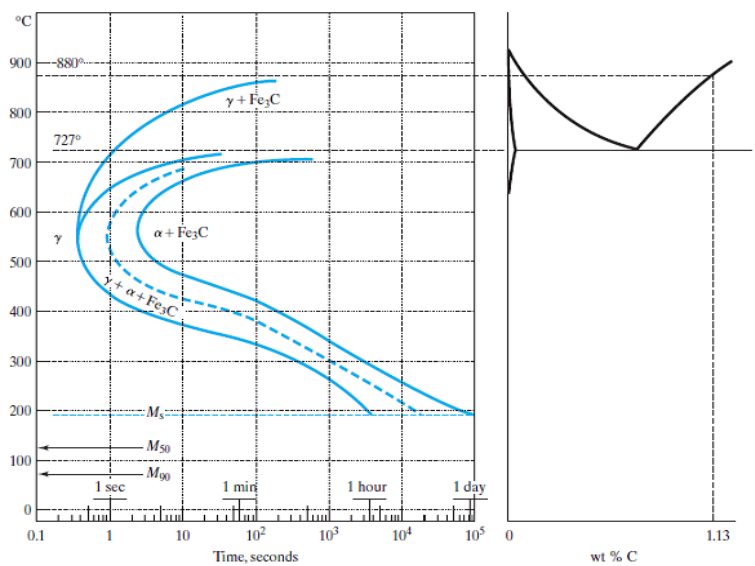

Figure 11 : *TTT Diagram for hyperetuctoid steel (0.8-2% C) [28]*

The prime objective of steel heat treatment is to achieve a suitable steel structure to meet a specific case. A particular design of the heat treatment process can help determine the steel's produced structure. Leading to an end product of a remarkable transformation from the innate position, which is the obtained structure. Through phase diagrams, such modifications are interpreted [20]. It is possible to research the crystal structures of austenitic transformation better at a specific temperature instead of by constant cooling. An iron-carbon phase diagram is by far the most helpful schematic for predicting several transition circumstances, but this does not get enough

detail on the steels' non-equilibrium state. They are usually called TTT diagrams or isothermal Transformation diagrams, explaining transitions underneath each scenario [21]. The ordinate is the temperature throughout this graph, and the resulting value seems to be the time graphed on a logarithmic scale.

In Figure 11, Hyper-eutectoid C2 compositions have a $\gamma+Fe_3C$ branch, identical to its hypo-eutectoid situation. We end up at $\gamma+Fe_3C$ for a temperature between T2 and TE [21]. For such a temperature below TE, we initially get the forming of pro-eutectoid Fe_3C leading to the formation of eutectoid $\gamma+Fe_3C$ [21].

2.4. Heat treatment

The important role of heat treatment is to dissolve all the carbides. It is vital to have an austenitic composition, carbide-free and completely homogeneous regarding both carbon and manganese. The original as-cast system should be free from segregation, gross inclusions, and pre-existing fractures to do this. In thick sections, the center is only partially transformed due to ineffective quenching. To decompose the $(Fe,Mn)_3C$, conventional heat treatment methods known as solution heat treatments are used [29]. The continuous carbides along with austenite grain limits and discontinuous carbides between austenite grains are seen in Figure 12. So, these carbides must be dissolved in the austenite matrix by soaking for sufficiently long periods at temperatures from 10 °C to 37 °C above A_{cm}. Grain growth can, however, occur under circumstances of that type.

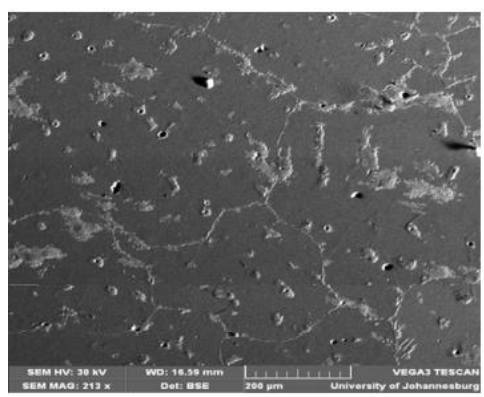

Figure 12 : *As-cast Hadfield steel showing grain boundary carbides [30]*

Heat Treatment process variables:

1. Temperature
2. Holding time
3. Heating Rate
4. Cooling Rate
5. Furnace Atmosphere

2.4.1. Importance of Quenching

It is an essential process that makes the steel non-magnetic, work-hardenable, resistant to impact and abrasive wear, tough, and admissibly cold-resistant in an optimal mode to form a homogeneous frame. Under industrial conditions, castings are solutionized at 1050-1150 ° C, and cooled in cold running water to have complete carbide dissolution and boost diffusion in austenitization [31]. When the Solutionizing temperature is increased to 1200°C in order to minimize the time of the total heat treatment period. The austenite grains in the casting expand, and due to superheating, carbides emerge [31].

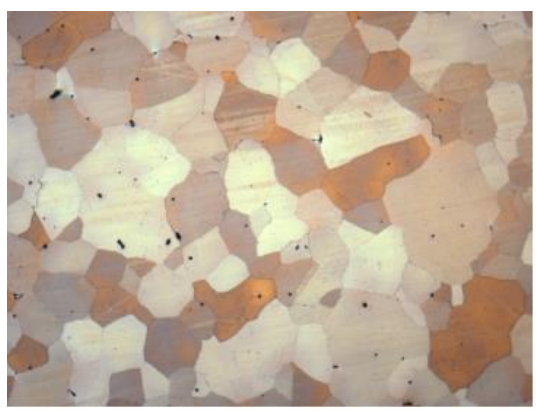

Figure 13: *Microstructure of properly quenched manganese steel magnified 100X [2]*

2.4.1.1. Quenching Mechanism

The choice of a cooling medium to harden the material relies on the cooling needed for the hardness to be desired. In order to understand the rate of cooling of any cooling or quenching medium, a standard curve of the kind must be studied, as shown in Figure 14. This curve illustrates the variations in temperature from the hardening temperature of the part being cooled or quenched. Cooling takes place in three discrete steps, each of which has unique rate characteristics, called A, B, and C [32].

As a part is quenched in a cooling medium, the role can almost instantaneously heat the cooling medium around it to the boiling point and vaporize the liquid. The region is surrounded (at stage A) by a blanket of vapor produced by the liquid. This further eliminates the cooling fluid from reaching the component's surface. Before forming a vapor coating, the surface layers of the part will be cooled very intensively.

Since the vapor envelope serves as an insulator, this slows down the cooling rate, and cooling happens mainly through radiation through the vapor film. The vapor-coating produced by the surrounding layers of liquid is constantly washed off [32].

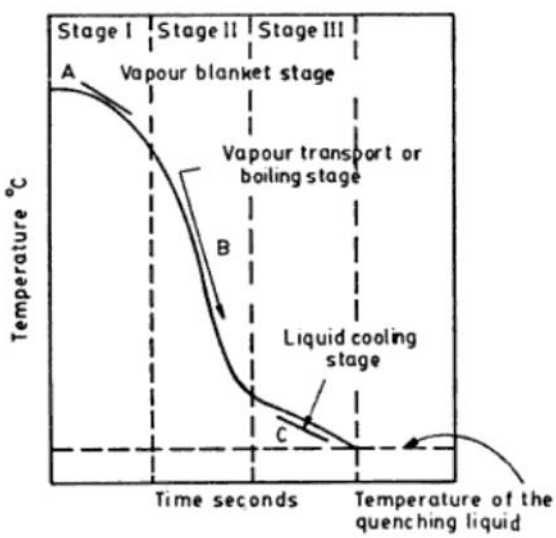

Figure 14: *Three stages of the normal cooling curve [20]*

The second stage B occurs as the component is further cooled, and the heat produced is not adequate to sustain a continuous blanket of vapor. The liquid has access to the part's surface at this stage, and a bubbling stream rises and disperses the vapor layer, resulting in a rapid cooling rate.

Once the boiling stops, the quenching liquid is in contact with all parts of the surface, the third stage, 'C' begins. During this stage of the process, cooling

is by convection; hence, the rate is sluggish. The cooling rate decreases as the metal's temperature drops.

The method to be followed for quenching is regulated by the grade of steel, section thickness, distortion permitted, and the properties to be imparted to the material. The different strategies for quenching are:

1. Direct quenching
2. Martempering
3. Austempering

2.4.1.2. Direct quenching

In this process, components kept for the necessary amount of time at the hardening temperature are directly quenched in water or oil to achieve the hard martensite structure Figure 15. The drawbacks to this approach are, firstly, the greater distortion and, secondly, the occurrence of cracks in the martensite range due to the very high cooling rate. This technique, however, is considered sufficient for mild steels, low-carbon, and medium-carbon steels [33].

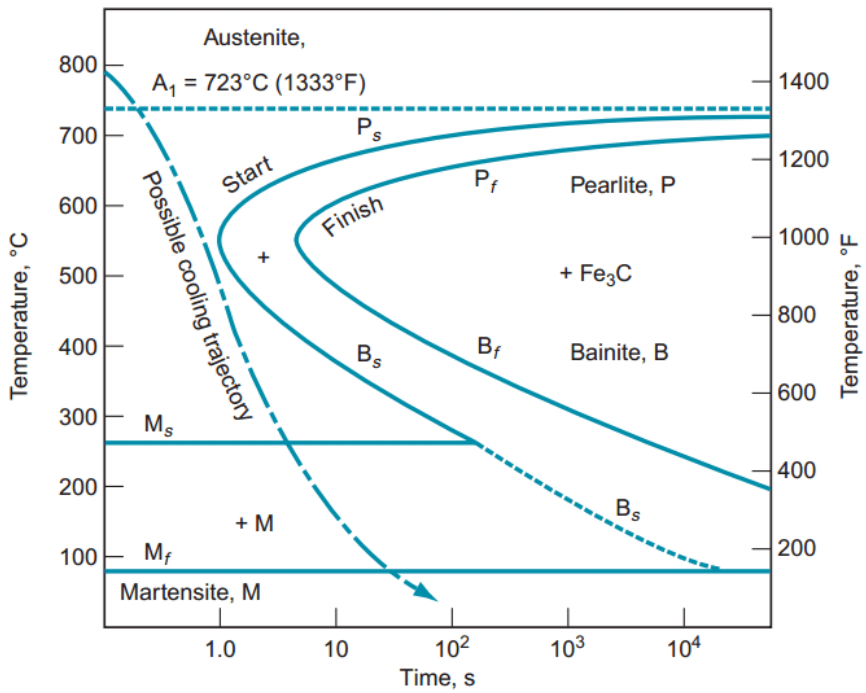

Figure 15: *TTT diagram indicating the temperature conditions on the surface and in the core of a specimen subjected to direct quenching [34]*

2.4.1.3. Martempering

Marquenching is the chosen name since martempering is not a method of tempering; thus, a false meaning is provided by the word martempering. It is a quenching process that is often used by certain alloy steels to increase ductility [35]. Generally,it is introduced after the steel has soaked at its austenitizing temperature. In this process, components are quenched into hot oil or molten salt from the austenitizing temperature just above the martensitic starting point of the treatment of steel Figure 16. The component is kept at this temperature until the components' surface, and core temperatures are about the same, but the component is not maintained long enough to turn into softer bainite [35]. If the quenchant temperature has reached the center of the component, the component is separated from the quenchant and allowed to cool in some suitable way (usually air cooling).

Due to uneven cooling between the middle and floor, this eliminates the creation of thermal stresses.

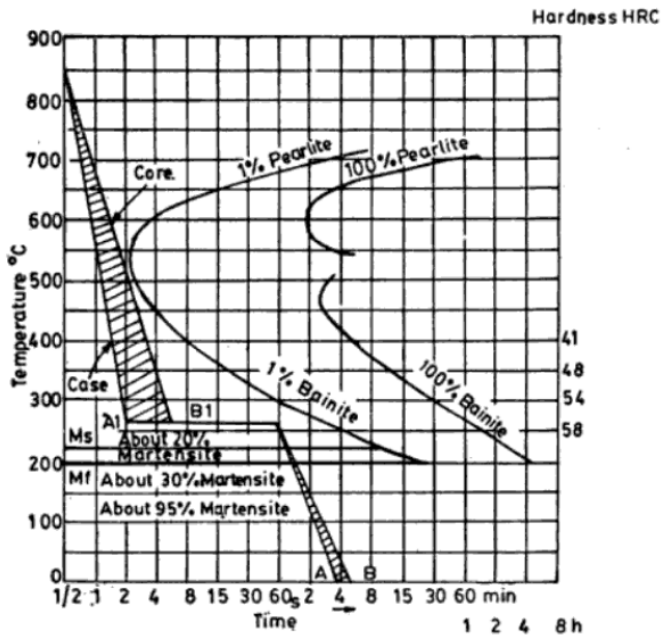

Figure 16 : *TTT diagram indicating the temperature conditions on the surface and in the core of a specimen subjected to martempering (Courtesy: Uddeholm Steel Corporation, Sweden) [20]*

Figure 15 and Figure 16, show the difference in the distribution of temperature on the component during quenching in water or oil as well as in the molten salt-bath held marginally above the steel temperature Ms. It is evident from Figure 15 that indirect quenching, the surface of the component is hardened before the beginning of the transformation in the center. The martensite structure starts to develop along the outside of the component when its temperature falls below the point where the Martensite forms and continues inside as cooling occurs until the temperature of the quenching oil pervades the portion. Martensite formation induces an increase in volume and a lack of ductility, first on the outside and then within a part [20]. This causes stresses that cause distortion and cracking.

The Effect of martempering can be seen in Figure 16. When compared to the transformation process discussed in 24. Before the martensite transformation starts, the temperature around the section reaches a constant value of that of the martempering bath A_1B_1. During the martensite transformation, internal stresses will grow and continue almost simultaneously in both the center and the case (thick and thin section) of the hardening portion. As a result, there is less residual tension, minimum distortion, and less chance of the component failing to quench cracks [36].

In order to harden a more comprehensive selection of steel, the martempering process may be further changed. The components are quenched 10-20°C below the temperature of Ms' in this process. This would speed up the component's running speed. Therefore, for hardening, a lower hardenability of steel can be introduced.

2.4.1.4. Holding time in the bath

Depending on the chemical composition, section thickness, temperature, and degree of agitation of the quenching medium, the holding duration in the heating bath varies. Bath agitation significantly improves the obtainable hardness [16]. The quenching in the hot bath must be continued until the entire portion reaches approximately the same temperature as the bath, in order to best exploit the benefits of heat treatment. Figure 17, offers an indication of the amount of time needed for this. This equalization time is somewhat independent of the hardening as well as the bath temperature under the cited limits [37]. As a consequence of the formation of bainite, prolonged holding time reduces the final hardness. The martempering time needed for temperature equalization in oil is approximately four to five times that required at the same temperature in anhydrous salt. The addition of 1 to 2% water to the molten salt results in the bath's efficiency.

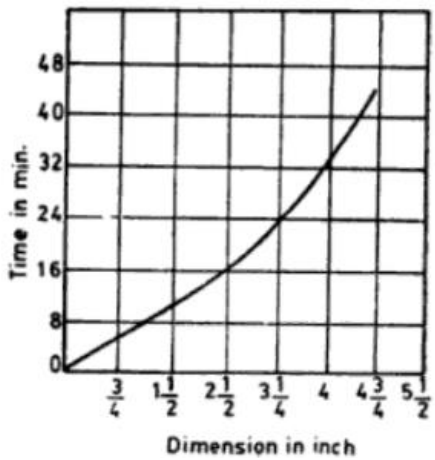

Figure 17 : *Least holding time required for the equalization of Temperatures in cylindrical steel specimens of various diameters [20]*

2.4.1.5. Aqueous salt solutions

When steel components are in use, they are subjected to stress, which necessitates varying amounts of mechanical resistance [38]. Because the qualities of steels are dependent on their structure, heat treatment enhances the hardening or even release of internal stresses are used in this class of materials, focusing at chemical and microstructural modification to maintain the authenticity of the component and its required functioning [38]. The hot metal is rapidly cooled by a medium (quenchant) from the austenitization temperature, which for Hadfield steel is usually in the range of 1000°C - 1225°C [39]. The two critical phenomena that occur during quenching that control the final metallurgical and mechanical properties of the components are heat transfer and wetting [40]. It is possible to change the surface of the cooling piece to disrupt the form of liquid vaporization or directly to the liquid vaporization process by introducing solutes to the quenching water [41] [38].We can see that increase in the concentration of the salt is directly proportional to the cooling rate and reduces the vapor blanket at 45°C [38]. Incorporating salt-forming solutions facilitated a more homogeneous cooling that maintained high heat flux values for the majority of the temperature drop. To prevent distortions and cracking during the quenching process, homogeneous cooling is preferred [38].

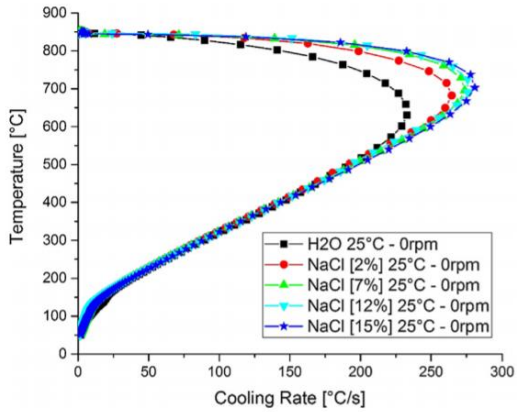

Figure 18: *Cooling rates curves for the aqueous salt solution of NaCl at 25 ℃. [38]*

Deformation twinning helps reduce the coefficient of strain hardening, implying that twinning is critical in steel deformation. Twinning nucleation stresses are predicted due to crystallographic orientations and the stress directions in the Hadfield steel single crystal [42] The following factors facilitate to resolve the kinematic barrier that prevents extrinsic stacking faults and twinning from forming: (i) the influence of applied stress on decreasing adequate extrinsic stacking fault energy including partial mobility, (ii) pile up dislocation stress concentration at the dislocation lock (iii) carbon atoms are trapped in a transient structure due to the passage of a leading partial (Suzuki effect), and Mn-C couples produce a short-range internal stress field [43].

2.5. Carbides

Carbides and embrittling transformation products are present in the steel in its as-cast state (Fe-Mn-C) [44]. The carbides develop when there is more than 1.0% C in the as-cast material or when alloying elements like Cr, V, Ti, and others are added. They form in heavy section castings throughout heat treatment if quenching is ineffectual in achieving quick cooling throughout the full section thickness, but they also form while cooling is exceedingly slow, regardless of mold cooling rates [45]. The existence and shape of carbides have a significant impact on the Hadfield steel's service properties, and because higher amount of carbides have an adverse influence on the Hadfield steel's service properties, considerable work has gone into creating techniques to mitigate their damaging consequences [45]. As a result, numerous parameters such as the chemical composition of the cast, casting circumstances, rate of solidification, micro-alloying components, and heat treatment cycles are being revealed as impacting carbide morphology in the steel [46]. The occurrence of carbides in the grain boundary or inside the grain has a negative impact on tenacity; modest amounts of carbides reduce the amount of energy to fracture toughness of austenitic manganese steel significantly. Its chemical composition, heat treatment, and dimensions all influence the lack of carbides [47]. Usually, there are two sets of carbides in the microstructure of Hadfield steel and are Primary carbides and secondary carbides.

(i) Primary Carbides: Carbides propagated during the solidification of steel are known as primary carbides, and they can be seen in most heat-treated steels. The usual particle size is observed in a few micrometers, and they are easily visible in the optical microscope. Because of their colossal particle size and great interparticle spacing, these carbides did not result in the steel's strength. Primary carbides were discovered to wear out at the same rate as the matrix, with abrasive tracks visible on the wear surface of primary carbides. Primary carbides may damage the steel because they behaved as abrasives, penetrating through the matrix and contributing to the observed high wear rate [48]. (ii) Secondary Carbides: Carbides accumulated during secondary hardening heat treatment of steels are known as secondary carbides. Secondary carbides are more difficult to comprehend from a

technical standpoint than primary carbides. The small particle size of these carbides, especially in the early stages of their synthesis, as well as their metastable character, makes evaluating them difficult [48].

2.5.1. Behavior of Carbides

During slow cooling or reheating over the 400-800 ° C range, the embrittling intergranular carbides in manganese steels type. They are extracted above 1000 ° C by solution annealing characterized by immediate quenching. The carbide formation kinetics follow the standard C-curve of an isothermal transformation diagram, with 600°C - 650 °C arising in the highest growth (carbide nose) [49].

There are two types of carbides form.

(i) Thin Carbide: These carbides shape very quickly and emerge in the engraved structure as grain boundary categorizations and viewed at the magnification level of 200-1000x. (ii) Thick Carbide: On thin carbides, thick carbides nucleate and expand along the borders of the grain. The thin carbides do not greatly embrittle the steel, while they severely embrittle the thick carbides [50]. Both are characterized on both sides of the cementite film by having a resolvable cementite interior with simple austenite or carbide interphase border [50]

Thin carbides are less stable, but with the austenite matrix, they have a strong lattice match [50]. This gives rise to an interface with low energy and a low barrier to nucleation. On the other hand, thick carbides are more stable constituents but have a greater energy interface and an elevated nucleation barrier [50].

Discontinuous, metastable thin carbides whose material is identical to Mn and Cr. The matrix nucleates rapidly at the boundaries of the grain. It consists of several discrete particles that give rise to the delineations in the etched microstructure detected. Anticipated to their small size and low energy, probably coherent, interface, these carbides have strong cohesion with austenite [50].

- The thick carbide thus produced is rapidly rising in a lateral direction in a continuous film, adding any thin carbides along its path along the grain boundary.

2.5.1.1. Effects on carbides with the rising temperatures

Selçuk Kuyucak et al. have proposed that the following mechanism operates for carbide precipitation during quenching [49].

- No noticeable changes occur up to around 400 °C in the composition of the steel. Fine needles (plates) of freshly developed carbides occur near the available carbides and around austenite grain boundaries at 450°C [50].
- The number of acicular carbides increases dramatically at 500 °C and reaches a height at around 550 ° C. Temperature development to 600-650 °C allows the length of the carbide plates to drop, but their thickness increases [50].
- More heating of the steel is not accompanied by qualitative changes in its structure but changes in the background around the carbides, i.e., the austenite becomes heavier, and the colour is closer to that of a fine dispersed ferrite-carbide mixture. The carbides begin to dissolve at 700°C clearly [50].
- At 800°C, carbides are conserved on the boundaries of austenite grains. The carbide remaining around the grains becomes thinner at 850°C. It splits and converts into individual chains at 900 °C, and the sizes decrease with further temperature rise. The iron-manganese carbides travel entirely into the solution at 950 °C [50].
- At last growth in the heating temperature and the lowering of the holding time influence carbide content and hardness of the metal [50].

The choice of the heating temperature of high-manganese steels for quenching depends on the carbon content (concentration) that can be derived from literature studies [51] [52].

- As the carbon content of the steel is increased, its impact resistance worsens at any preferred heating temperature for quenching (t_q).
- The impact intensity reduces the most when the carbon content in the steel is ≥ 1.20 % and t_q > 1150 °C.
- In the case of quenching from 1250 °C, beginning with 1.20% C, the sensitivity of the steel to lower the impact hardness is the highest, which is demonstrated by the presence of superheating austenite over the grain boundaries and within grains, and of fine laminar carbides over the crystallographic.
- In steel quenched from 1150 °C and consisting of 0.95 to 1.15% carbon, the highest impact hardness was found.
- High-carbon manganese steel of carbon content (1.25 %) is also susceptible to the forming of hot and cold cracks (especially > 1150 °C quenching)

Although the carbon content of 1.30% in high-manganese steel is very close to its ultimate solubility in austenite, it can be expected that the higher the carbon content in the casting, the greater the risk of developing residual carbides in the austenite structure in traditional modes of heat treatment of this steel. In our view, the carbon content of not less than 1.20% -1.30 % should be recommended for high-manganese steels working in abrasive wear conditions (attrition). The carbon content should be limited to 0.90%-0.95%if the castings of this steel are exposed to substantial impact or static loads (excavator ladle teeth, crusher jaws, railway spider cores, etc.). [30]

With the allowance for reduced thermal conductivity of high-manganese steels and a significant factor of linear expansion compared to the same characteristics of carbon steels, it is essential to slowly (especially up to 700-750 °C) conduct heating of steel castings for quenching. Accelerated heating from 500 to 750 °C produces significant internal pressures capable of creating cracks [53]. Depending on the thickness of the walls and the mass and configuration of the castings, castings are usually charged into the heat-treatment furnace at a temperature of 300-550 °C in the working room of the furnace. At this temperature, the castings are held in the furnace for 1.5h to 2h.

The holding time of the castings is determined by the thickness of their walls and depending on the rate of dissolution of carbides in the austenite, which usually ranges from 1 to 8 h [54]. In the process of quenching the castings, the water temperature in the quenching tank should not exceed 60 °C; otherwise, if the cooling rate is inadequate, the metal of the castings acquires not only carbide but also martensite. The higher the temperature of the water in the quenching tank (with respect to the optimal value), the lower the casting hardening depth would be. It is unfavorable to repeat heat treatment (quenching) of high-manganese castings, particularly in the case of their complex geometry, with the intention of dissolving the retained carbides (after initial quenching), as this would lead to a significant increase in rejection (up to 70 %) due to quenching cracks. [55]

2.6. Defects

I. **Microporosity:** Austenitic manganese steels have a wide cooling range [49]. Consequently, the formation of microporosity is a frequent characteristic in these castings, independent of loading. Microporosity appears as random pockets in clusters [49]. The development of microporosity is primarily influenced by gaseous solute concentration, oxide inclusion concentration and distribution, and solidification rate (pouring temperature, molding medium, usage of cooling, and sheet thickness) [49]. As oxide inclusions are widespread after the steels are once heat-treated, the gaseous solute concentration and solidification rate are likely the most relevant [48]. Moreover, microporosity arises more often in interdendritic locations, and its grain boundary fraction is substantially higher than its volume fraction [48].Indeed, the grain boundary fraction of microporosity constituents increases in brittle property in this steel

II. **Inclusions:** Steel inclusions are usually the result of normal deoxidation and desulfurization processes [56] (i) After removing carbon, the next step is to eliminate or make less dangerous dissolved oxygen and sulfur, which, if left in solution, would precipitate as low-melting-point iron compounds, making the steel weak and unworkable at high temperatures [57]. When considering inclusions as pitting initiation sites, it's important to remember that they're not just inactive debris. Still, they are precipitates seeking thermodynamic equilibrium with the steel in which they have previously been dissolved. (ii) Because of the presence of the high chromium concentrations in stainless steel, the reactions differ thermodynamically from those when compared to carbon steel. The reactivity of oxygen and sulfur is reduced, making them more soluble [56] [57].

3. Methodology

In the chapter, we will look through the methodologies used for carrying out the experimentation and the analysis. The sequence will be as followed, Heat treatment Processes, sample cutting, sample preparation, followed by the material characterization using Optical Microscopy, SEM, and EDS. The microstructure will be investigated along with the mechanical properties of the samples

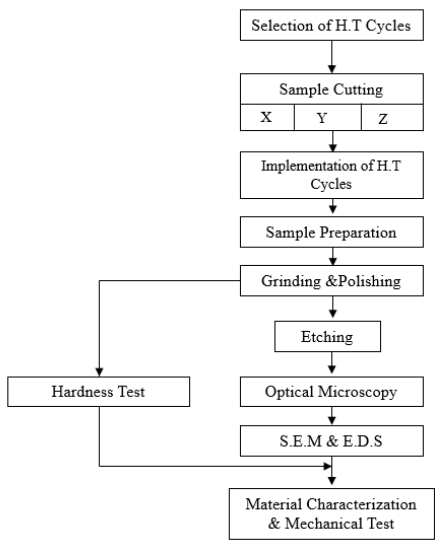

Figure 19 : *Schematic representation of the experementation*

3.1.1. Materials

As mentioned, Hadfield steel was used in the experimental portion of three different compositions, i.e., X, Y, and Z. They were initially manufactured and machined in the sizes of 290*72*22mm blocks. Each steel grade's block was further categorized to acquire samples of appropriate size for further hardness analysis. Twelve samples from each grade of each plate were cut using Wire-Electric Discharge Machine EDM (Brother HS-50A), as requested, and the measurements were 25*25*22mm (L*B*H) dimensions. The sectioning of the same can be seen in Figure 20.

Table 2: *Identification and compositions of Steels*

Designation	C %	Mn %
X	1,10-1,23	10-13
Y	1,35-1,45	15-18
Z	1,38-1,47	15-18

As mentioned in Table 2, three manganese steel grades were used in the experimental portion of the investigation—the first, grade X, which has a lesser number of alloyed variants except for %Cr. An increase in the Chromium results in a further increase of wear resistance of the material. Grade Y, and the third, grade Z, have a higher alloyed variant than grade X. It is important to highlight the compositional differences between grades (X, Y, Z). Grade Z has a higher Manganese (Mn), Carbon (C), and Chromium (Cr) content. And so, it is expected that these samples are compositionally different enough that one can assign differences in behavior to their composition.

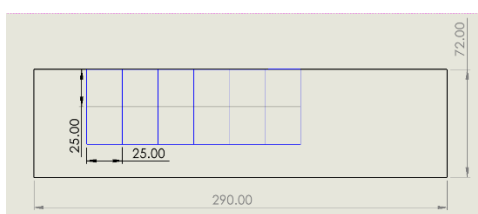

Figure 20: *Dimension of samples and region of cut section (blue lines).*

3.1.2. Heat Treatment Process

To investigate the results of various heat treatment parameters on the grain boundaries and hardness, five heat treatments were conducted on all three steel grades. These are characterized by a steady heating ramp up to the desired temperature, a holding time at that temperature, followed by rapid quenching in water solution, and different compositions of salt solutions. The following heat treatment cycles were selected/formulated based on the literature study and the datasheets, as shown in Table 3.

Table 3 : *An overview of the applied heat treatment cycles and sample naming.*

Sl. No	Heat treatment Process	Sample code	
HT 1	Slow Heating (500°C - 800°C) 2H – (900°C-1200°C) 1H – W.Q A	X – D Y – C Z – B	
HT 2	Initial Heating (150°C -450°C) Slow Heat (1000°C-1300°C) – Salt Quench 1%-2% and 2%-4% NaCl	1%-2% NaCl	2%-4% NaCl
		X – HT	X – NL
		Y – IT	Y – OL
		Z– LT	Z – XL
HT 3	Initial Heat (150°C - 440°C) -Slow Heat (800°C - 1140 °C),1.5 H – Heat (800°C - 1140 °C), 2H – W.Q. A	X – E Y – F Z – G	
HT 4	Preheating to (500°C-800°C), 10H – Heat to (800 °C-1100°C), 2H – Water quenching	X – MH Y – LSH Z – ISH	
HT 5	Slow Heat (500°C - 900 °C),at the rate of 120/hr, 2H – Heat (900 °C-100°C), 2H –Water + Salt Quenching	1%-2% NaCl	2%-4% NaCl
		X – S	N
		Y –R	O
		Z – T	P

A Kejia Furnace-KJ1600T, laboratory furnace with a PID furnace controller was used for the heat treatments, as shown in Figure 21: Kejia Tube Furnace. Every furnace trial included one sample from each designation (X, Y, and Z), and the samples were placed approximately 2 mm from one another to ensure that they experienced the same heating as seen in Figure 22. Each heat treatment was programmed according to the desired cycle, further giving inputs to the furnace. Samples were then quenched into a container according to the HT cycle requirements. After every heat treatment, the container was cleaned, and a new stream of water was introduced. The temperature of the water was checked and kept at room temperature. Totally, 27 Samples were Heat Treated.

Figure 21: *Kejia Tube Furnace*

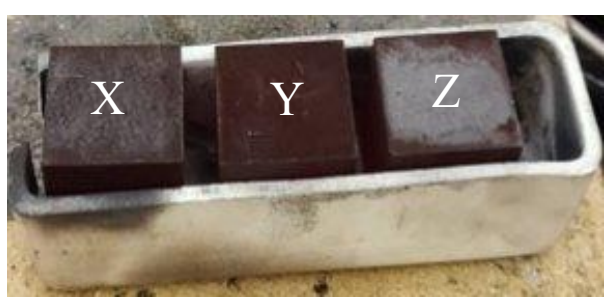

Figure 22 : *2mm gap between samples*

3.1.3. Heat Treatment cycle

Since the new heat treatments were meant to represent those that are done at an industrial level, a standard was set to establish differences in heating rates and timescales. The primary purpose of these new heat treatments is to improve the grain boundaries by having less carbides around them, which will further result in higher impact toughness and improve the mechanical properties. Figure 23, gives the comparison of the experimental heat treatment cycle used for this thesis.

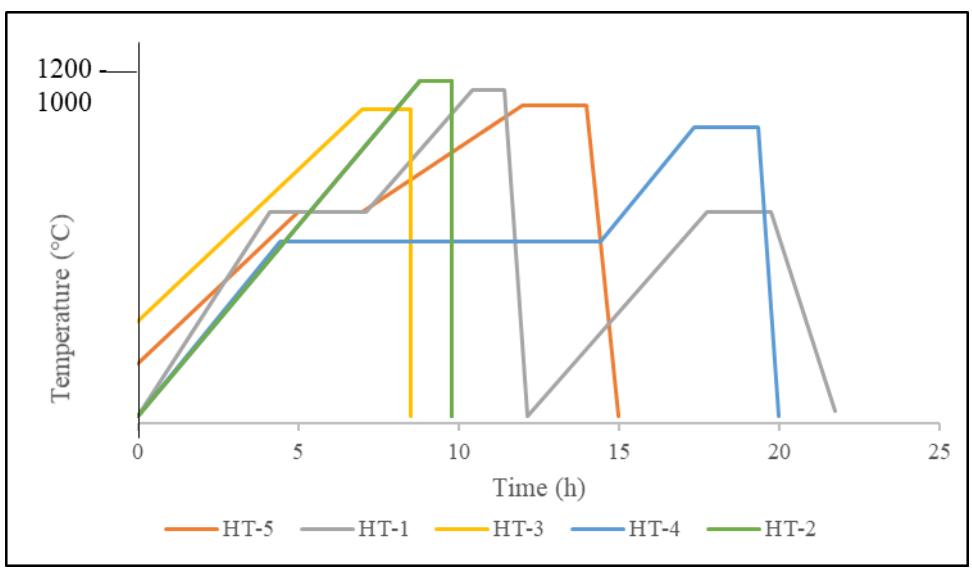

Figure 23: *Comparison of the experimental Heat Treatment Cycles*

3.1.3.1. Heat Treatment Cycle – 1 (Aging)

The first stage of the cycle involves heating samples to the range of 500°C - 800 °C at the rate of 100°C/hr and held at this temperature for two hours. Further, reheating to austinization temperature of 1000 °C-1100°C /hr and held for 1hrs. The samples were then quenched in agitated water at room temperature. The second stage involves reheating to 600 °C-800°C and holding for 2hr. Finally, the samples were left for air cooling until it reaches

room temperature. The schematic design of the heat treatment cycle is shown in Figure 24.

The research conducted by *Keyur Panchal* provides us information about aging or precipitation hardening, which will improve by carbide inclusion around the grain boundaries in and around microstructure, eventually improving the wear resistance of the Hadfield steel [58].

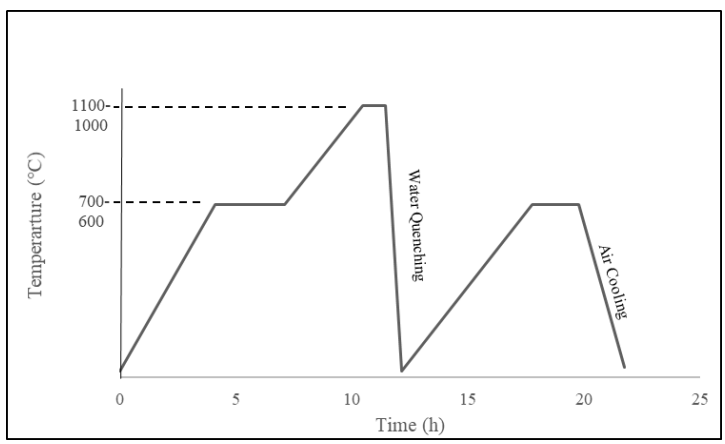

Figure 24 : *Heat treatment cycle - 1*

3.1.3.2. Heat Treatment Cycle – 2

This cycle involves heating up to the austenitization temperature range of 900 °C-1300 °C at the rate of 100°C/h followed by holding at respective temperature for 1hrs. Then the samples are quenched in the solution of 1%-2% NaCl and 2%-4% NaCl, under room temperature. The schematic design of the heat treatment cycle is shown in Figure 25.

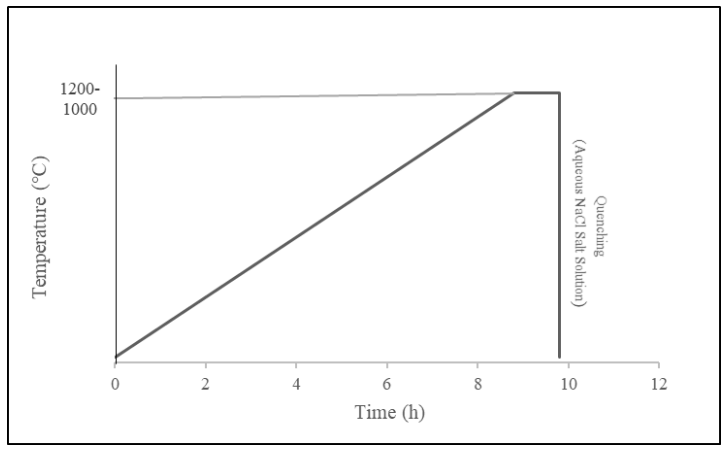

Figure 25: *Heat treatment cycle - 2*

3.1.3.3. Heat Treatment Cycle – 3

The cycle involves preheating the furnace to 150°C -450°C. This was followed by slow heating at the rate of 100 °C/hr, until it reached the austenitization temperature range of 800°C-1200°C and held at this temperature for 1.5 hrs. Finally, the samples were quenched in agitated water at room temperature. This technique is also called quench hardening, The microstructure from the water-quenched samples has well-defined austenite grain boundaries, which can be attributed to hardness values, and the impact strength is enhanced by the absence of carbides both on grain boundaries and grains as per Ibitoye et al [59]. The schematic design of the heat treatment cycle is shown in Figure 26.

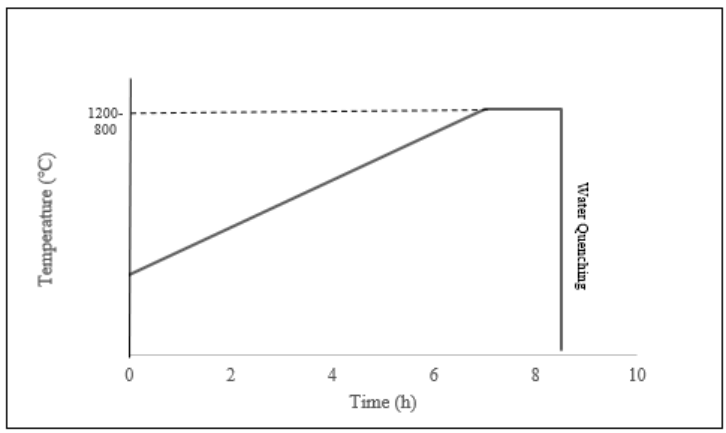

Figure 26 : *Heat treatment cycle - 3*

3.1.3.4. Heat Treatment Cycle – 4

This cycle involves heating samples to 500°C-800°C without any heating rate and holding them at that temperature for 10hr. Further, they were heated again to the austenitization temperature range of 800°C-1100°C and held for two hours. Lastly, the samples were quenched in the water at room temperature. From the study conducted by Hidayat and Bandanadjaja, with the use of pro isothermal heating, we can improvise the toughness for this type of steel, especially for the grade Z [29]. The schematic design of the heat treatment cycle is shown in Figure 27.

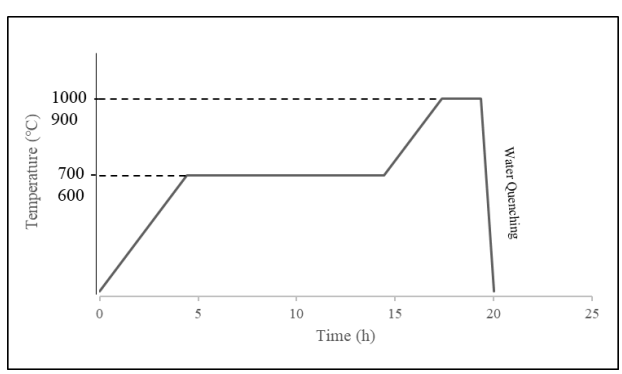

Figure 27: *Heat treatment cycle - 4*

3.1.3.5. Heat Treatment Cycle – 5

This cycle involves heating the samples to 500°C-800°C at the rate of 100°C/hr and held at that temperature for 2hrs. Further, the samples were heated again to 900°C-1300°C and stored at that temperature for 2hrs followed by two different quenching solutions as follows:

- Solution with 1%-2% NaCl
- Solution with 2%-4% NaCl

The schematic design of the heat treatment cycle is shown in Figure 28 : Heat treatment cycle - 5 The (2%-4% NaCl) solution quenched samples were eliminated from the microscopy study due to the corrosion on the sample's surface, but the hardness test is conducted after cleaning the surface with Acetone.

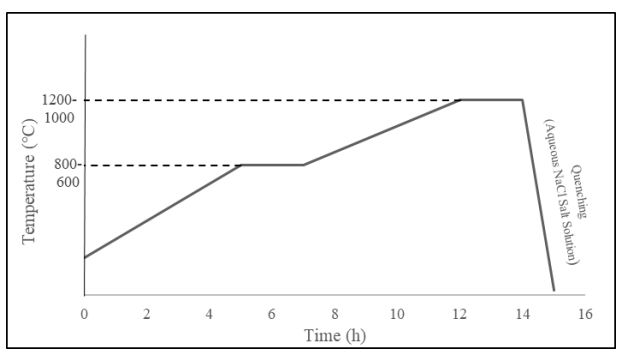

Figure 28 : *Heat treatment cycle - 5*

3.1.3.6. Heat Treatment Cycle – 6

This cycle involves heating the samples to a range of 500 ºC-700°C within 1hr. Then the samples are held for 2hrs at the range of 500°C-900°C, further cooled in the air until the room temperature. Then the sample is heated up to the austenitization temperature range of 900°C-1300ºC again and stored within 2hr at that temperature, and finally quenched in agitated water. The heat treatment graph is shown in Figure 29. Interestingly, this cycle is eliminated from further study and Table 3. Because, while experimenting,

we came across the formation of corrosion on the prepared samples, which made it challenging to analyze.

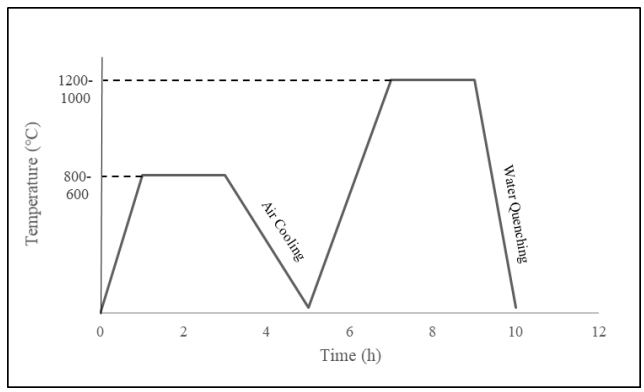

Figure 29 : *Heat treatment cycle - 6*

3.1.4. Sample Preparation

3.1.4.1. Hot Mounting

For the metallographic investigations, a small piece from the heat-treated samples was mounted by the embedding device called as Struers Citopress-5, shown in Figure 30 (A). CitoPress is a robust hot mounting press with high speed and user-friendliness for quick turnaround and higher productivity. All the samples were hot mounted in a Polyfast compound. Figure 30 (B) shows the parameters used for each hot mounting process. The applied pressure was 325 bar at 180 °C, for 3.5 min. The cooling process took 1.5 min with the water. Therefore, the total process took 5 min for each sample.

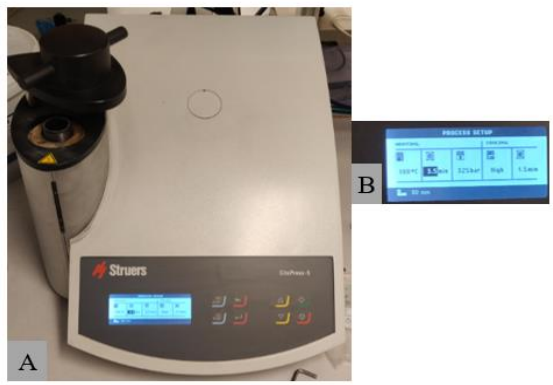

Figure 30 : *(A) Struers Citopress-5 (B) Parameters for hot mounting*

3.1.4.2. Grinding and Polishing

Once the samples were hot mounted, A Struers Tegramin semi-automatic grinding and polishing machine was used for this process. A five-step grinding process was performed to have a smooth surface by using a typical grinding cycle, and mounted samples were initially grinded using a grinding disc with a grit size, followed by polishing as mentioned in Table 4, using water as the lubricating and cooling media. MD-Piano is a resin bonded diamond surface designed and developed for plane grinding and fine grinding materials [60]. It should also be noted that the rotational speed was 300 rpm, and the pressure was in the range of 25-30 N for all grinding steps.

Figure 31 : *Struers Tegramin-25 [60]*

Besides, a several-step polishing process was done using the suspensions mentioned in the table. The polishing was achieved by using a series of micro cloths and suspensions with a more acceptable particle size every time concerning the rotation of the samples.

Table 4 : *Sequence of the steps for grinding and polishing.*

Step No.	**Surface**	**Suspension**	**Lubricant**	**Force** (N)	**Rotation Speed** (rpm)	**Time** (min)
1	MDPiano 220	-	Water	25	300	5
2	MDPiano 500	-	Water	25	300	5
3	MDPiano 1200	-	Water	15	300	5
4	MDPiano 2000W	-	Water	15	300	5
5	MDPiano 4000W	-	Water	10	300	3.30
6	MD Plan	DiaPro All/Lar 9 µm	-	10	180	5
7	MD Dac	DiaDuo 2-3 µm	-	5	180	3
8	MD Nap	DiaDuo 2-1 µm	-	5	180	5
9	MD Chem	OP-U Non-dry	-	5	200	1.30

3.1.5. Material characterization

3.1.5.1. Metallographic investigation

The metallographic investigation is performed according to the ASTM E3-11 for the preparation of the samples. As we know, the preparation of samples for critical microscopic examination is complex. Great care should be taken to avoid cold working and disturbed surface layers. Cold worked scratches from early stages may be flowed over and concealed during fine

polishing, only to become pronounced after etching. Similar flow may obscure grain boundaries whose character is an essential criterion of the quality of heat treatment. Spurious structures may also result from tarnishing and corrosion caused by the atmosphere.

The surfaces of all the 21 polished samples having a similar 30 mm diameter were etched according to the ASTM 407-07, with Nithal [**2% Nitric acid (HNO_3) + 98% Alcohol (CH_3OH)].** When the sample was etched, they were rinsed with water (2 beakers of water, transferred one to another) then with the alcohol. Finally, the sample was dried under the hot air gun and were covered with caps to protect the surfaces.

The samples were then examined under Alicona InfinteFocus optical microscope further after selection of the best heat treatment cycles. Only nine samples were further analyzed scanning electron microscope (SEM), Tescan Mira3 High-Resolution Schottky FE-SEM, which is equipped with Energy Dispersive (EDS) and with the resolution of 1.5 nm under the voltage of 15 kV was used at the Department of Geology at Lund University. In addition, (EDS) mapping and spot analysis were also done; analysis was made to identify each type of carbide, mapping the grain boundary distribution on these samples.

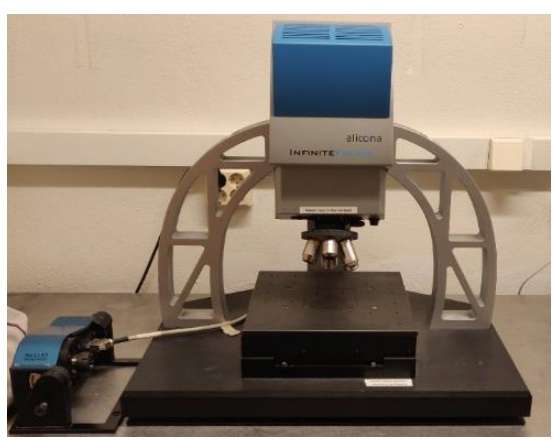

Figure 32 : *Alicona InfinteFocus Optical Microscope*

Figure 33 : *Tescan Mira3 High Resolution Schottky FE-SEM [61]*

4. Results and Discussions

In this chapter, the results from the implemented Heat treatment cycles and examinations will be presented. Including the composition and concentration of carbides along the grain boundaries and the microstructure, the hardness of the material, and the variation of chemical composition in the carbides of different regions. Photographs of the microstructure structure of the material samples and typical patterns observed after the heat treatment and the type of quenching medium used, which will be further followed by the discussions.

4.1. Results

All the specimens were studied under the optical microscope. The selected samples were then subjected to comprehensive SEM examinations to obtain information about the surface topography. Finally, EDS analysis was performed to identify the elemental composition of materials.

4.1.1. Microstructural Results

This section gives information about the grain boundaries of each grade when subjected to various heat treatment cycles. The figures are arranged according to different magnifications (high to low) and compared accordingly.

i. Heat treatment - 1

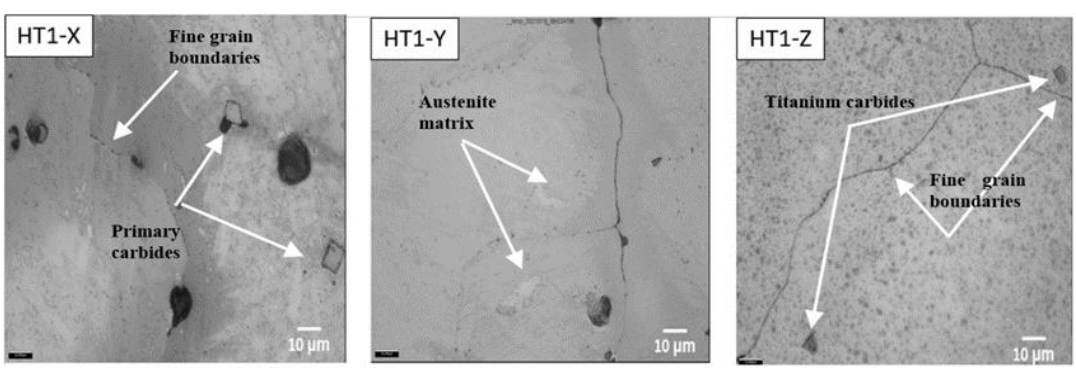

Figure 34 : *Microstructure of different grades at 100x magnification*

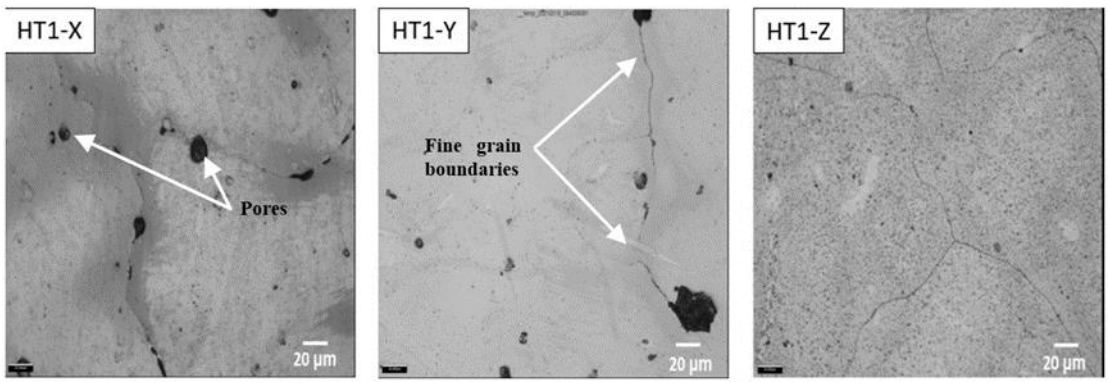

Figure 35 : *Microstructure of different grades at 50x magnification*

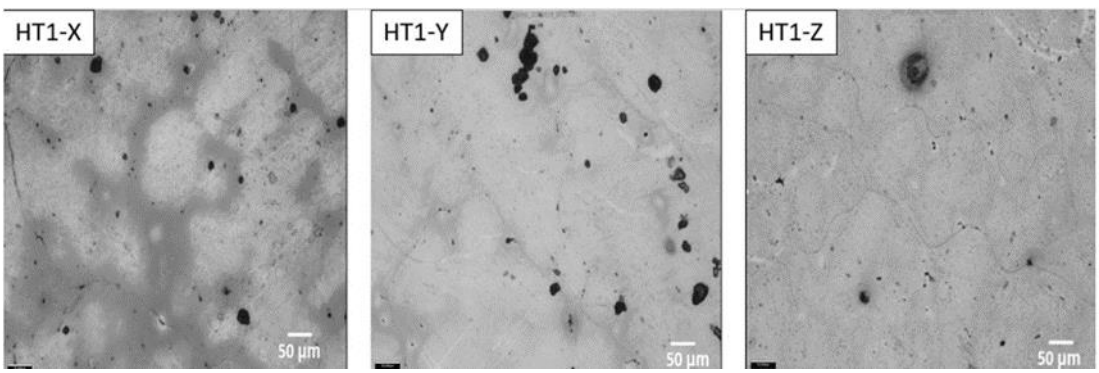

Figure 36: *Microstructure of different grades at 20x magnification*

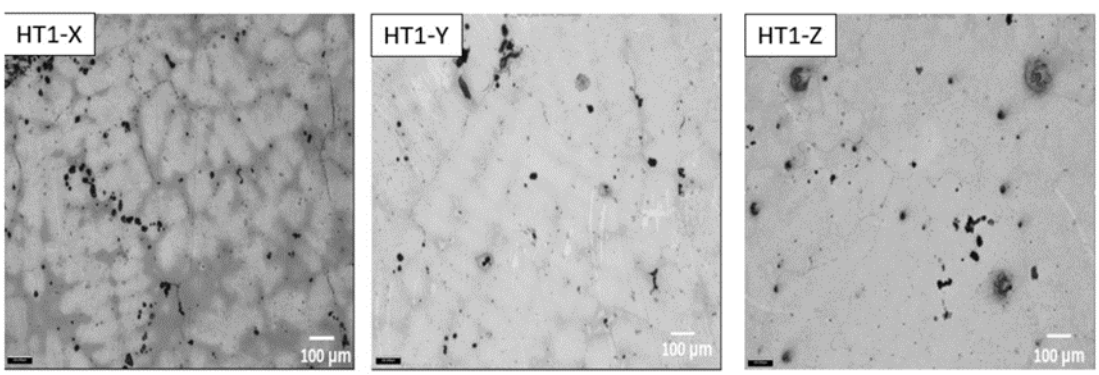

Figure 37 : *Microstructure of different grades at 10x magnification*

(Figure 34-Figure 37), show the optical micrographs of the three different steels use. As seen in these figures, all three analyzed steels have an austenitic matrix and are free from the residues of alloyed cementite at the grain boundaries. The enlarged images of the grain boundaries, carbides are shown at top, Figure 34 and Figure 35. The investigation confirms that the grain boundaries carbides of HT-1-Z steel grade are more refined than those of HT-1-X and HT-1-Y steel. There are significantly fewer carbides on grain boundaries in an austenitic matrix. The images also give information about pores present in three different steel grades. From Figure 36, we observe more pores in HT-1-X and HT-1-Y than in HT-Z. Surprisingly, the most crucial point to be considered is the presence of titanium carbide (Figure 34,Figure 35) on the grain boundaries and in the austenitic matrix. Because of its fine microstructure, the HT-1 microstructure is more promising in mechanical properties that could lead to high ductility.

ii. Heat treatment - 2A (1%-2% NaCl)

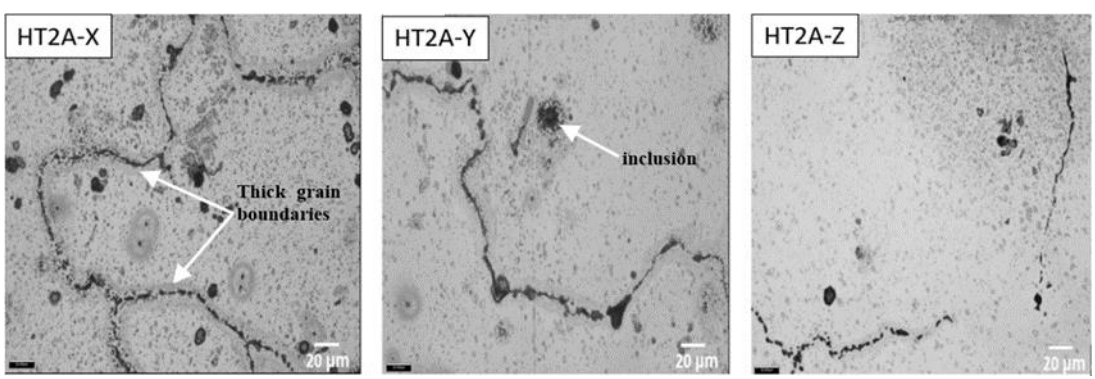

Figure 38 : *Microstructure of different grades at 50x magnification*

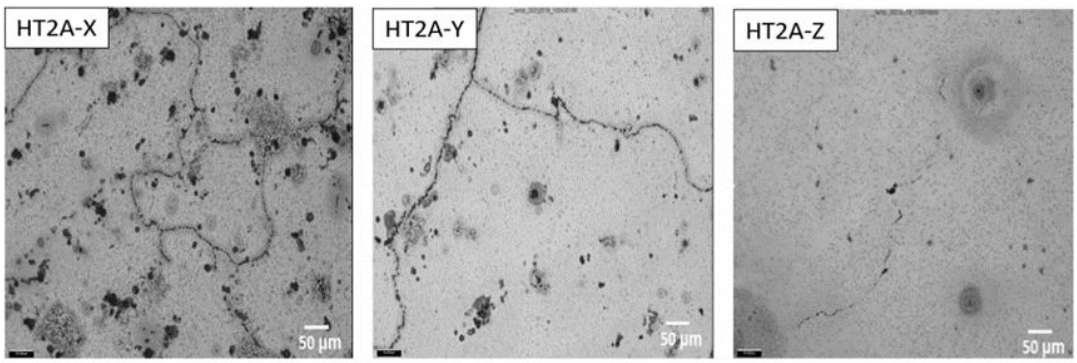

Figure 39 : *Microstructure of different grades at 20x magnification*

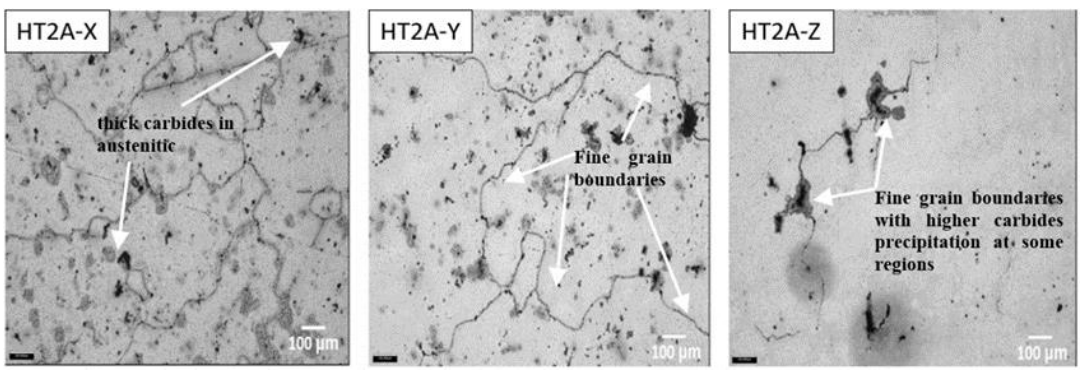

Figure 40 : *Microstructure of different grades at 10x magnification*

Microstructures obtained for sample heating at the range of 900 ℃-1300 ℃, followed by quenching in 1%-2% NaCl solution, are presented in (Figure 38,Figure 40) for 1.5hrs holding time. Compared with different steel grades at additional magnification (Figure 38Figure 40) large carbides and denser grain boundary carbides are visible after quenching in the 1%-2% NaCl solution. The sample of steel grade HT-2-Z presents a more significant (finer) quantity of grain boundary carbides than compared with the HT-2-X Figure 39, further followed by significant grain boundaries carbides of sample HT-2-X. Also, a higher carbide concentration in the microstructure (rise of the carbide/matrix ratio) is noticeable in Figure 40.

iii. Heat treatment -2B (2%-4%NaCl)

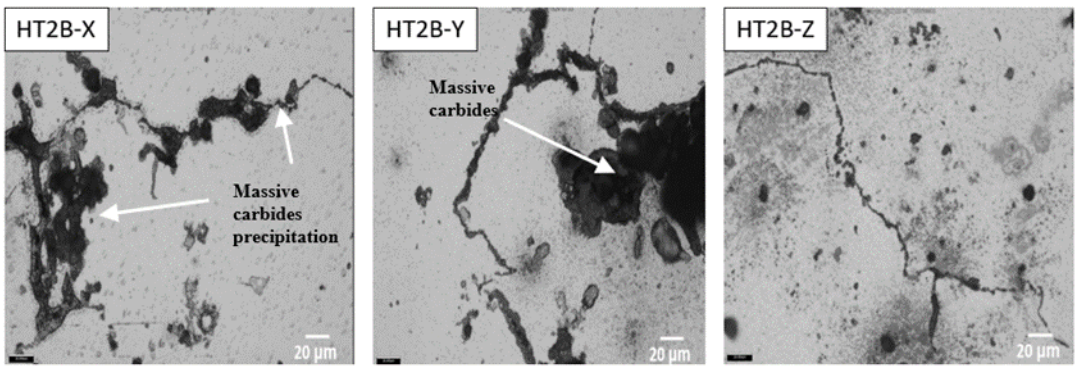

Figure 41 : *Microstructure of different grades at 50x magnification*

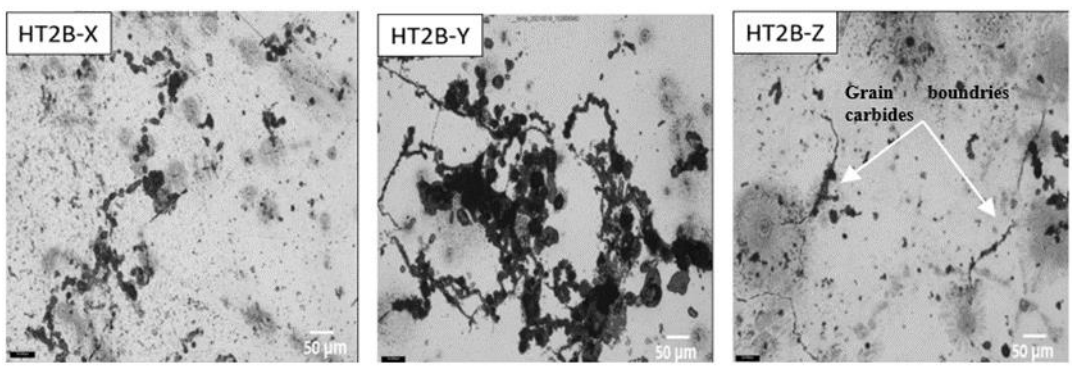

Figure 42 : *Microstructure of different grades at 20x magnification*

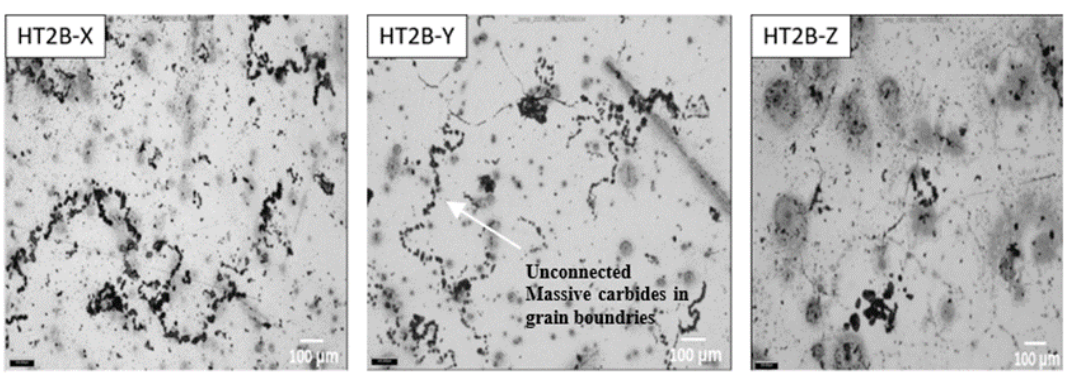

Figure 43: *Microstructure of different grades at 10x magnification*

As observed in the figure, all the three studied steels have an austenitic matrix, and secondary carbides precipitated at the grain boundaries. Figure 41, describes the microstructure of samples composed of massive carbides precipitation and are structured as individual islands and networks at grain boundaries and in an austenitic matrix. As shown in Figure 43, there are unconnected massive carbide islands dispersed into each grain in the HT-2B-X and HT-2B-Y steel grades. The carbide networks produced at grain boundaries can enhance material intergranular corrosion and embrittlement. HT-2B-Z has thinner grain boundaries as compared to the other two steel grades (Figure 41). However, the massive unconnected carbides are still present.

iv. Heat treatment - 3

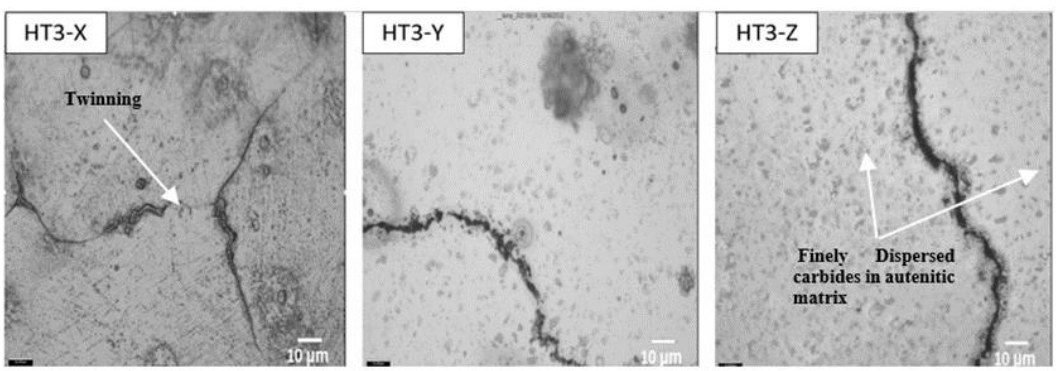

Figure 44 : *Microstructure of different grades at 100x magnification*

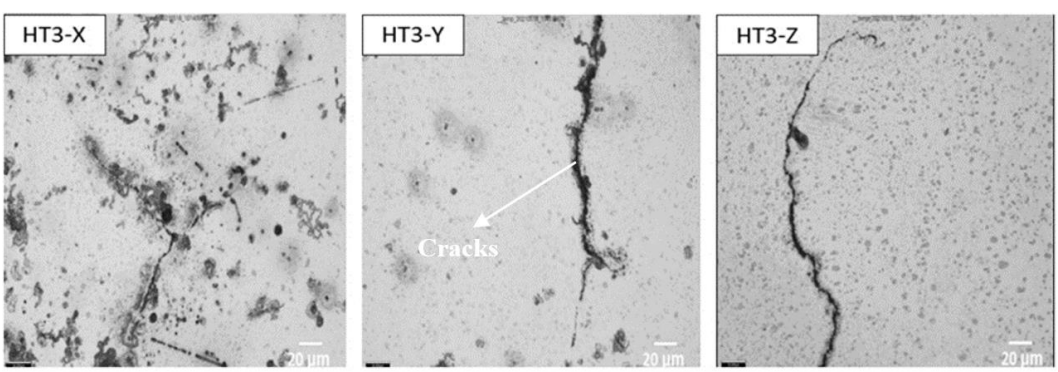

Figure 45 : *Microstructure of different grades at 50x magnification*

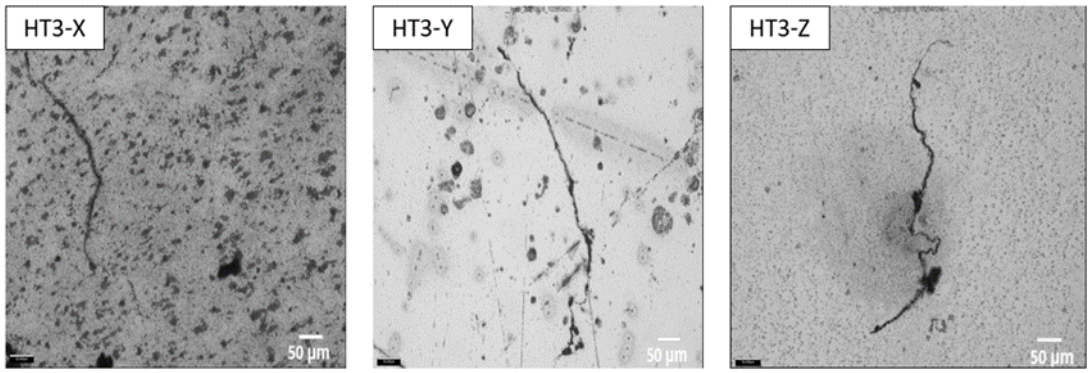

Figure 46 : *Microstructure of different grades at 20x magnification*

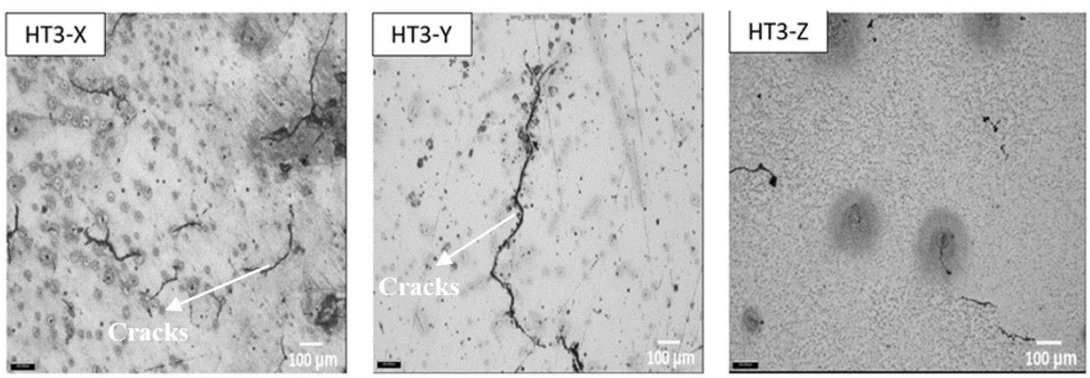

Figure 47 : *Microstructure of different grades at 10x magnification*

There are carbides (Figure 44) distributed homogeneously within the grains of all three steel grades HT-3 (X, Y, Z). The microstructure in all three steel grades shows carbides (black constituents) sparsely dispersed in the austenitic matrix. The homogeneous distribution of the carbides is clearly revealed in microstructures images obtained for the sample. Astoundingly, cracks were found on the samples. The investigation shows the presence of twinning in grade X (Figure 47). We shall also observe that the microstructure of grade Z has finely dispersed carbides around the austenitic matrix and has fewer pores than grade X and grade Y (Figure 47).

v. Heat treatment - 4

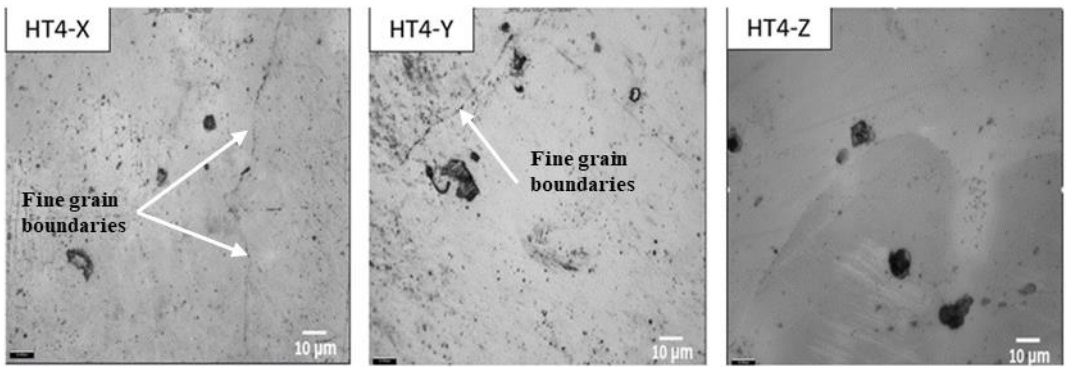

Figure 48 : *Microstructure of different grades at 100x magnification*

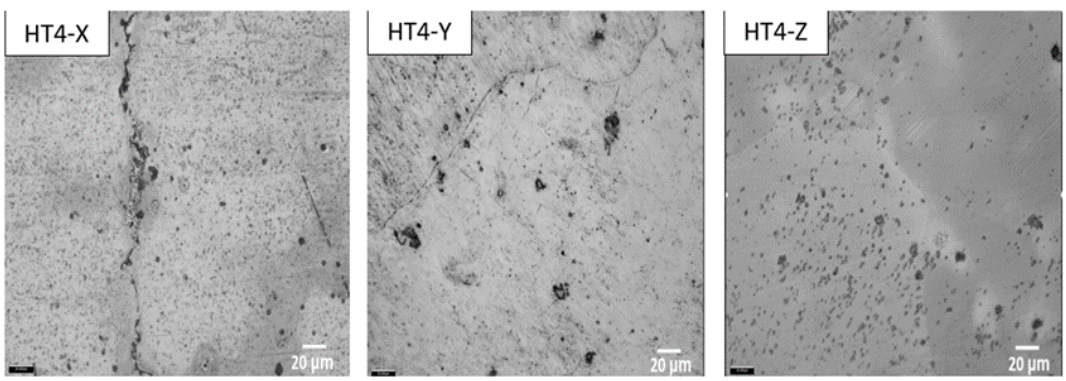

Figure 49 : *Microstructure of different grades at 50x magnification*

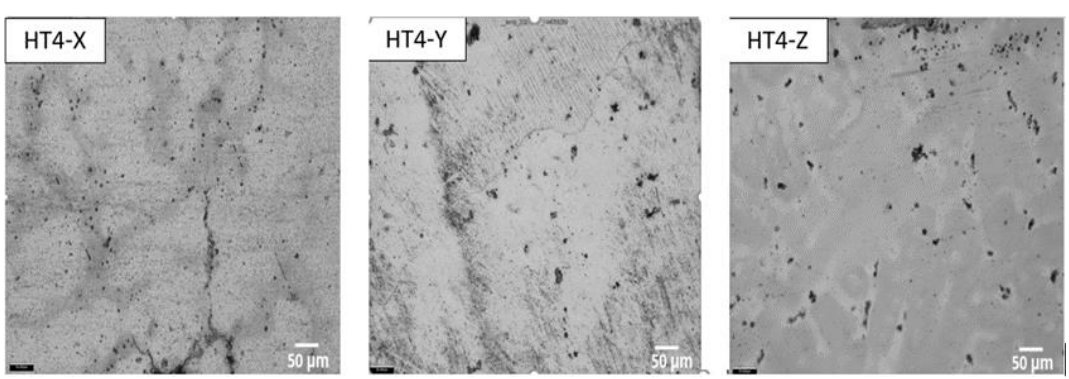

Figure 50 : *Microstructure of different grades at 20x magnification*

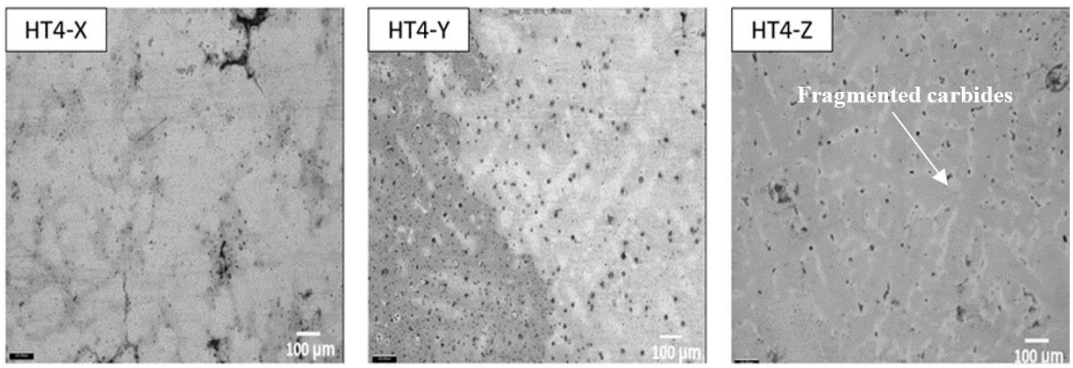

Figure 51: *Microstructure of different grades at 10x magnification*

The microstructures presented in (Figure 48, Figure 51) show a significant result compared with the samples subjected to water quenching. Finely dispersed carbides in the austenitic matrix are visible, as we can see at higher magnifications (Figure 48). The microstructure of steel grade HT-4-Y and HT-4-Z shows austenitic grains (Figure 51) with very thin grain boundary carbides, almost disappeared. However, steel grade HT-4X has few thicker carbides in some regions (Figure 49, Figure 51).

vi. Heat treatment-5 (1.5%NaCl)

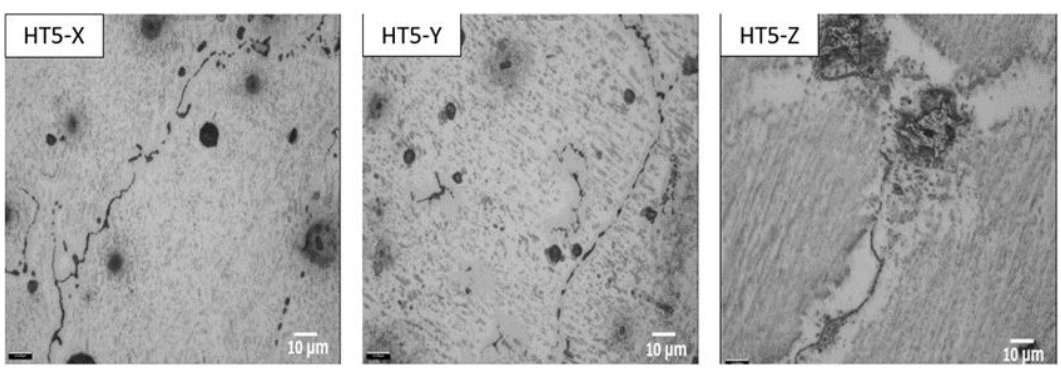

Figure 52 : *Microstructure of different grades at 100x magnification*

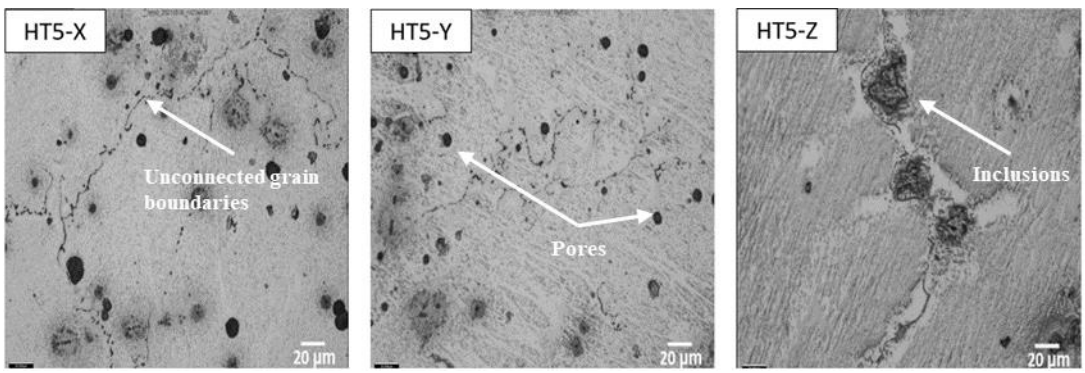

Figure 53 : *Microstructure of different grades at 50x magnification*

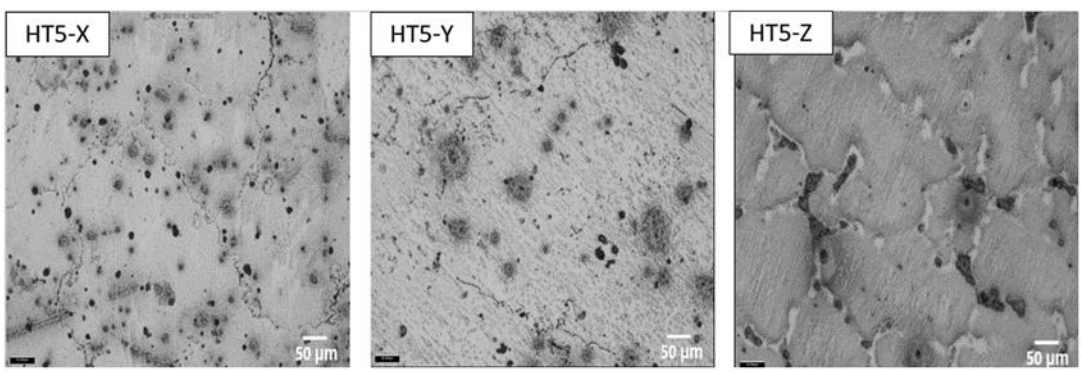

Figure 54 : *Microstructure of different grades at 20x magnification*

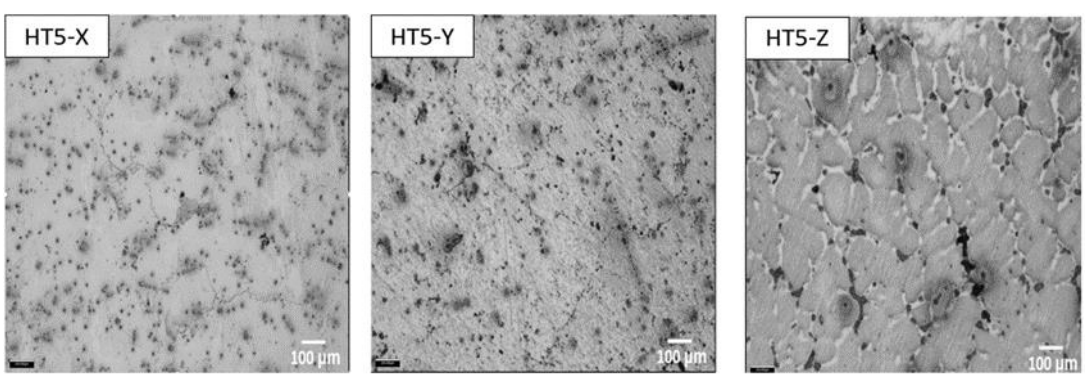

Figure 55: *Microstructure of different grades at 10x magnification*

The microstructure of three steel grades, X, Y, and Z, at different magnifications, is shown in (Figure 52-Figure 55), respectively. In this case of Heat treatment, the presence of a lower amount of carbide was observed in all three grades. In addition, for grade Z, when observed from a lower magnification of 10x, carbides have dispersed in the austenite matrix, and sulfide inclusions surrounded some carbides. The microstructure shows the unconnected carbide islands dispersed into austenitic matrix and grain boundaries for grades X and Y. When the salt was added to the water, inclusion appeared on the surface of all three steel grades, as shown in (Figure 53, Figure 54). However, the inclusion size was increased in the quenching solution that contained an amount of salt, which was not suitable for mechanical properties.

4.1.2. Selection of samples for SEM AND EDS analysis

From the above microstructure information, SEM and EDS analysis has been performed for selected heat treatment cycles. After all the 21 samples were heat-treated, each heat-treated sample was individually inspected in the optical microscope to see if the heat treatment cycles have been successful. Several heat treatments have demonstrated deformations such as significant cracks, large pores, and inclusion. Where else, other samples were heat-treated perfectly. These selected heat treatment cycles resulted in a suitable microstructure with fewer carbides around the grain boundaries and an austenitic matrix. Therefore, it would make sense to focus and make a primary selection of which heat-treated samples should be further analyzed and characterized. Such a selection is crucial for two main reasons. One, this thesis is time-restricted, and the focus is on good results. Second, as explained earlier, the main aim is to achieve a perfect heat treatment cycle for given steel grades, which yields an ideal grain boundary that further results in good mechanical properties like ductility and strength. However, if a studied heat treatment yields in a bad microstructure having massive and precipitated carbides, the heat treatment is already failing to meet the primary goal. However, the tight time frame that this project is running on does not allow for that. Thus, the focus is on the best heat-treated samples with fewer carbides around grain boundaries and austenitic matrix. In total, nine samples

were analyzed in detail in which 4 of each grade (X,Y, and Z) were chosen. Below are the selected heat treatment cycles.

1. HT-1
2. HT-2 (1%-2% NaCl solution)
3. HT-3 (Z)
4. HT-4 (X, Z)

4.2. SEM and E.D.S Results

4.2.1. SEM analysis

4.2.1.1. SEM analysis of HT-1

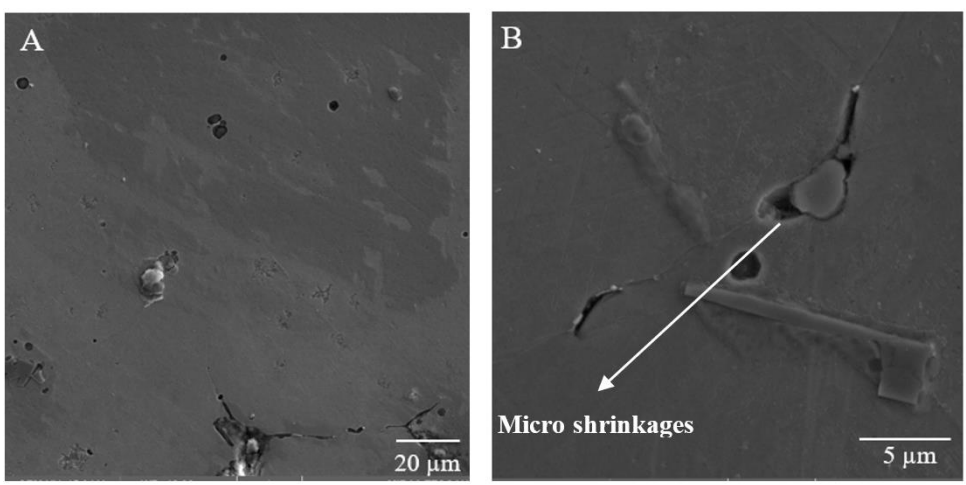

Figure 56: *(A).(B) SEM images of sample X*

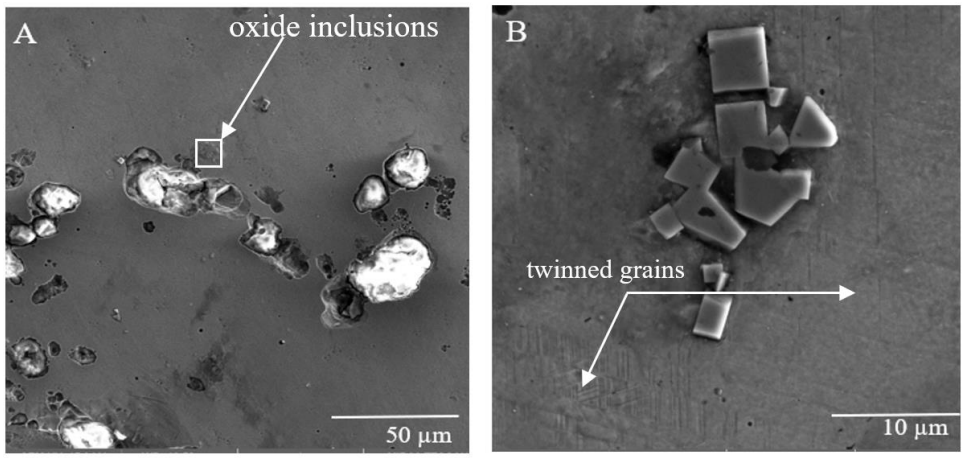

Figure 57 : *(A),(B) SEM images of sample Y*

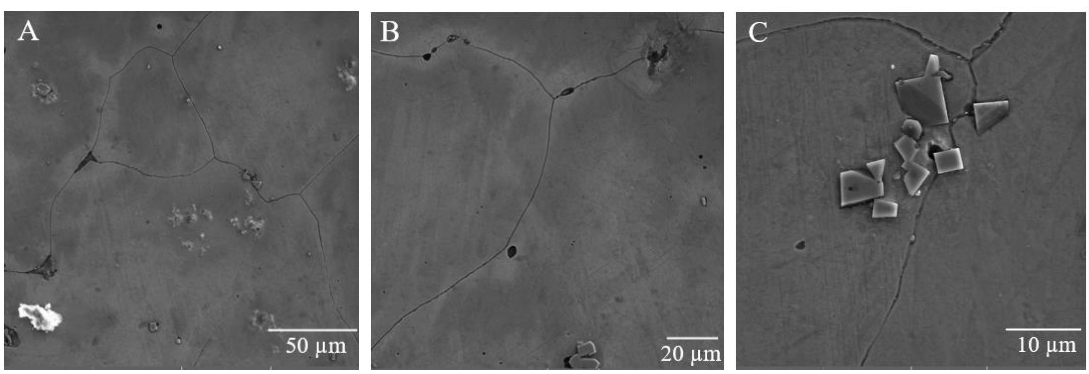

Figure 58 : *(A - C) SEM images of sample Z*

(Figure 56, Figure 58) provides us the details about the SEM analysis of grade X, Y, Z heat-treated under condition 1 (HT-1) as seen in Table 3. A small amount of carbide precipitation in the grain boundaries was noticed for grades X and Y.

From Figure 58, we can observe that grade Z has acceptable, clear-cut grain boundaries compared to the other two grades. In addition, the presence of

titanium carbide is visible in grades Y and Z, which can be seen in Figure 57 B, Figure 58 B.

4.2.1.2. SEM analysis of HT-2 (1.5% NaCl)

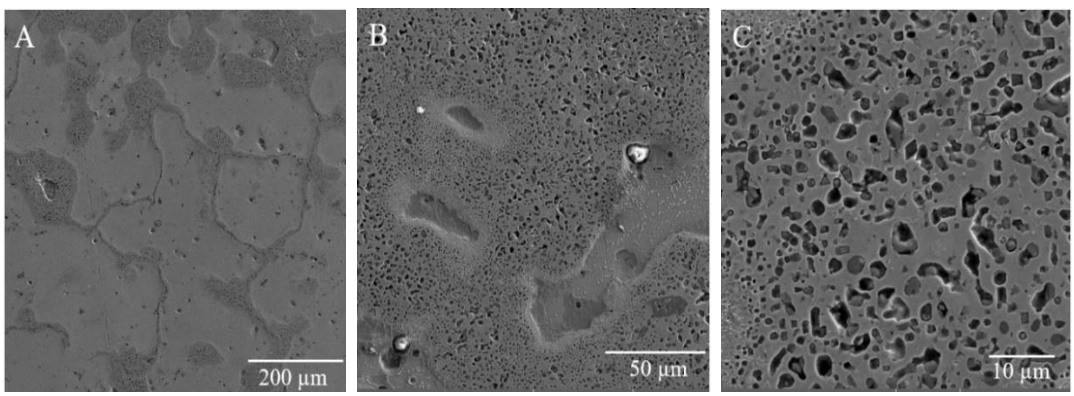

Figure 59 : *(A - C) SEM images of sample X*

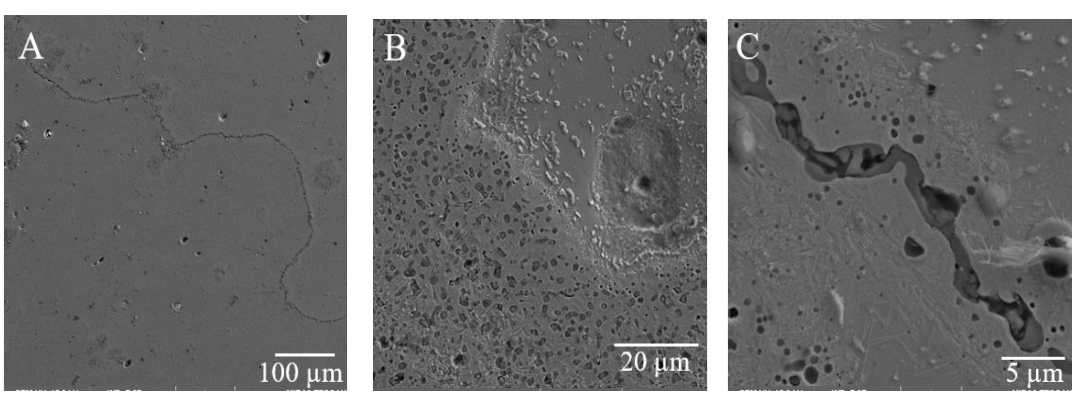

Figure 60 : *(A - C) SEM images of sample Y*

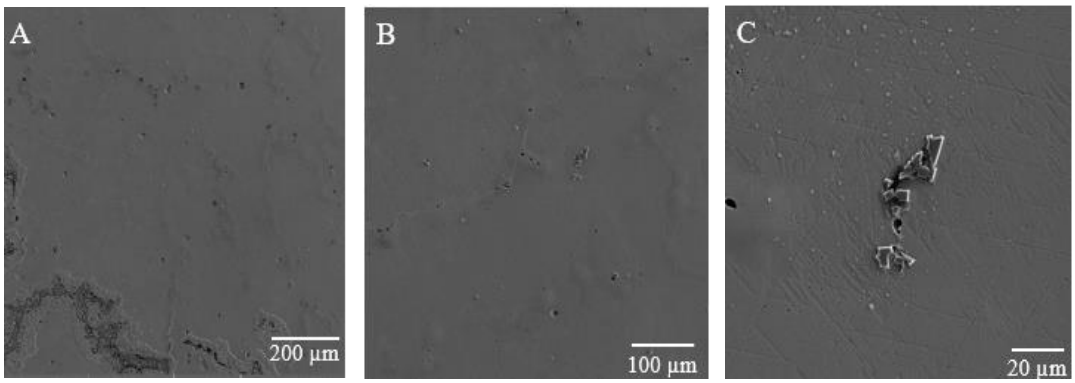

Figure 61 : *(A - C) SEM images of sample Z*

Figure 59 shows the higher precipitation of carbide in the grain boundary. In Figure 60-(C) the presence of massive intergranular carbide was recognized. Also, it is essential to notice the existence of pores in the austenite grains. Figure 61 shows secondary carbides in the grain boundary were not identified. However, primary titanium carbides were observed in grade Z.

4.2.1.3. SEM analysis of HT-3

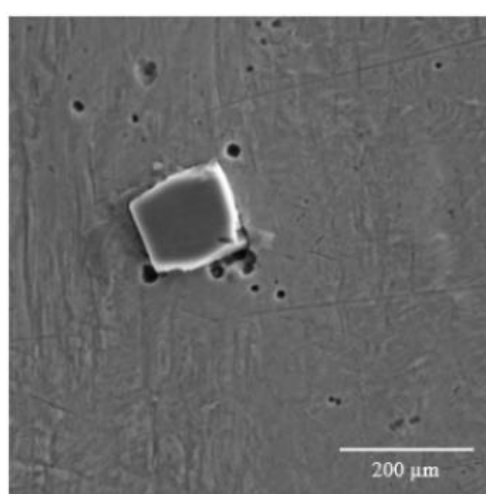

Figure 62 : *SEM image of Z*

Figure 62, shows us the presence of primary carbide(titanium carbide) and a homogenous austenitic matrix containing few pores around the primary carbide. Due to the challenging time, SEM analysis was performed only on grade Z, as one of the primary focus was towards material Z due to its high carbon and chromium content.

4.2.1.4. SEM analysis of HT-4

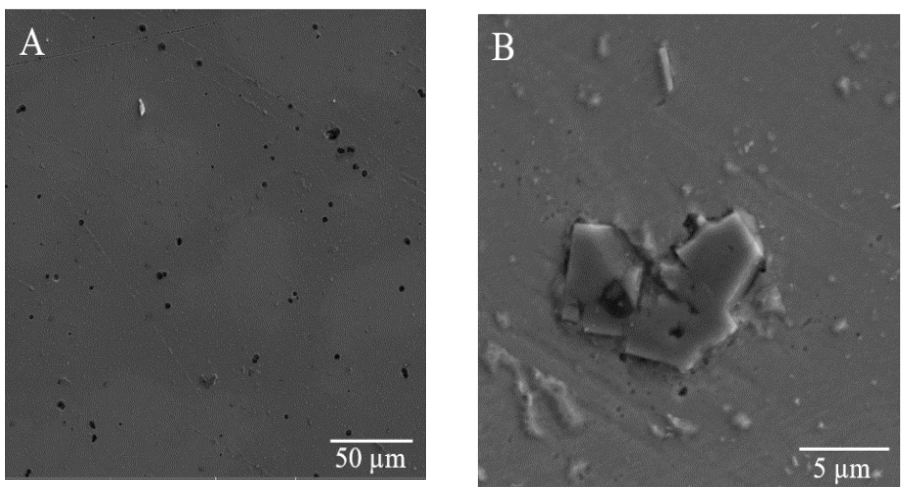

Figure 63 : *SEM images of sample X*

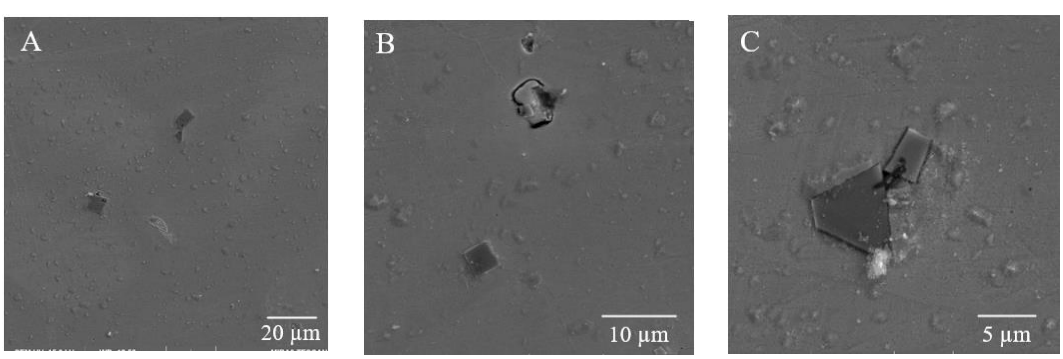

Figure 64 : *SEM images of sample Z*

(Figure 63, Figure 64) gives the detail about the SEM analysis performed on all three grades X, Z. Figure 63, shows no carbide presence in the grain

boundaries. However, a heart shape primary titanium carbide structure was visible in an austenitic matrix of grade X, Figure 63 (B). We see no grain boundaries, although primary titanium carbide was visible in Figure 64 (A, B, and C).

4.2.2. E.D.S Analysis

4.2.2.1. E.D.S analysis of HT-1

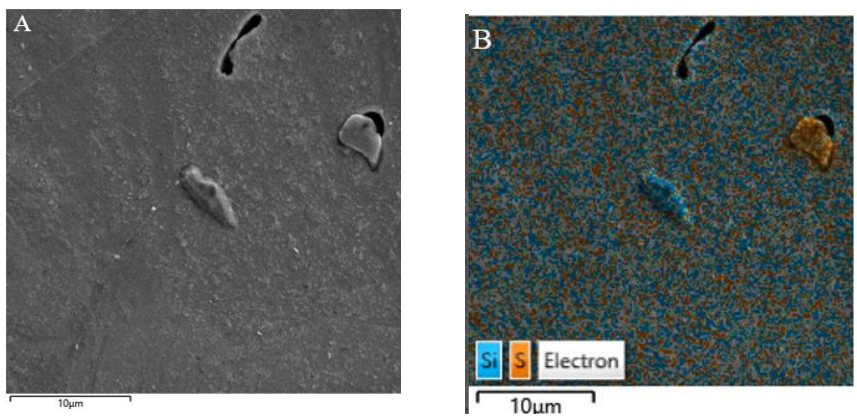

Figure 65 : *(A) SEM image of a carbide found in the top area of the surface material X. (B) EDS Layered image*

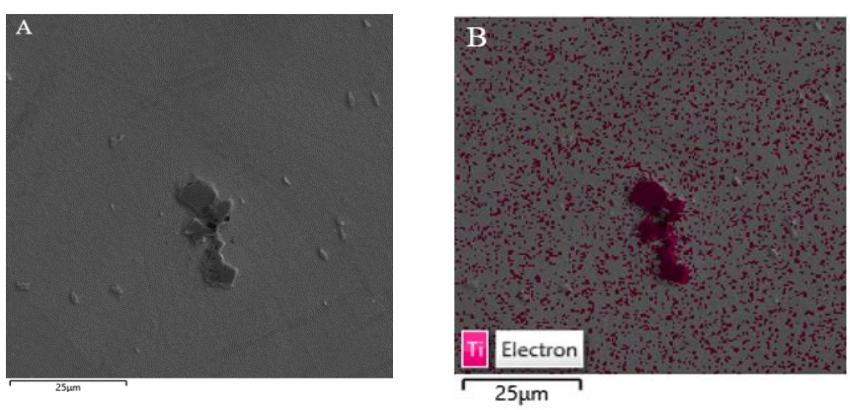

Figure 66 : *(A) SEM image of a carbide found in the top area of the surface material Y. (B) EDS Layered image*

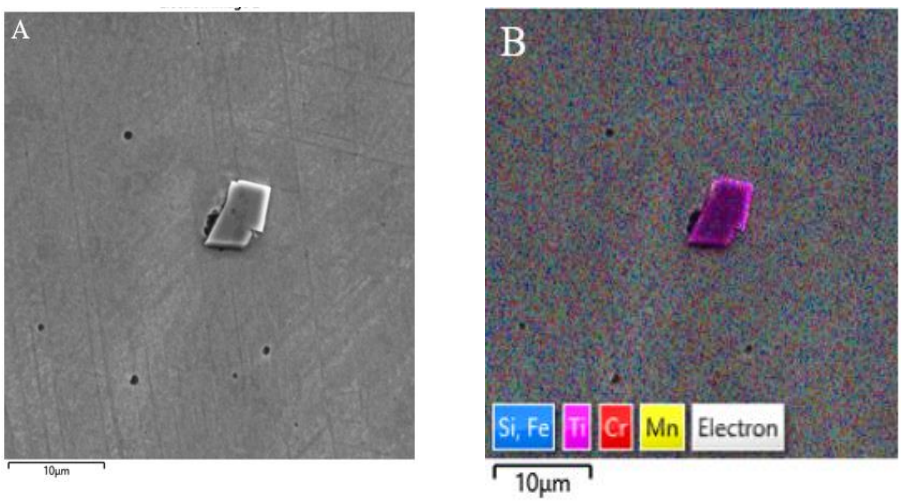

Figure 67 : *(A) SEM image of a carbide found in the top area of the surface material Z. (B) EDS Layered image*

The results of the Energy-dispersive spectroscopy (EDS) analysis of grade (X, Y, and Z) heat-treated under HT1 condition are as shown in (Figure 65-Figure 72), in which (B) indicates the EDS layered image, which includes the austenitic matrix, and the carbide. Both sites were analyzed and compared with each other. In Figure 65, the presence of sulphur as primary carbide was observed following titanium as primary carbide in Figure 66 and Figure 67. For grade Z, there was homogenous dispersion of silicon, iron, chromium, and manganese compositions in an austenitic matrix.

4.2.2.2. E.D.S analysis of HT-2 (1.5% NaCl)

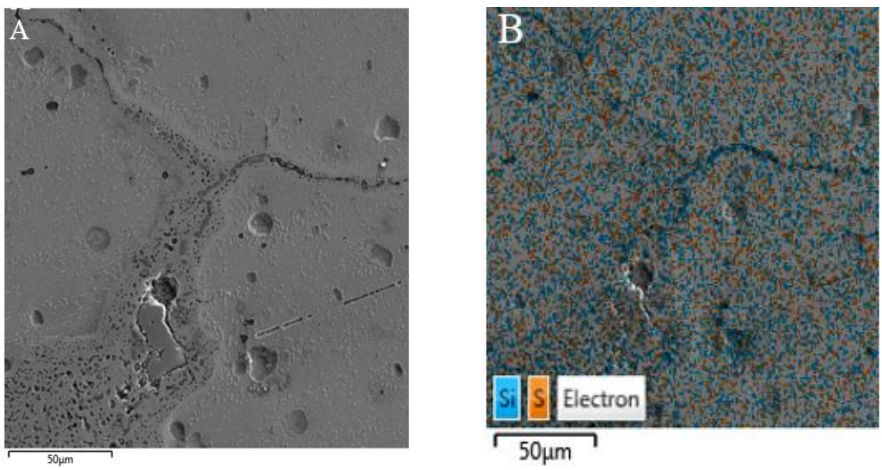

Figure 68 : *(A) SEM image of a carbide found in the top area of the surface material X. (B) EDS Layered image*

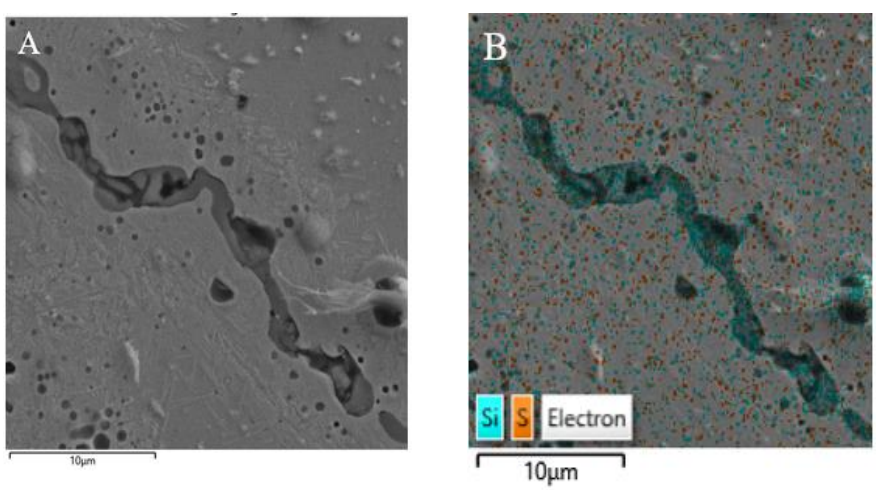

Figure 69 : *(A) SEM image of a carbide found in the top area of the surface material Y. (B) EDS Layered image*

The investigation of the Energy-dispersive spectroscopy (EDS) analysis of grade (X, Y, and Z) heat-treated under HT2 condition are as shown in Figure 68, Figure 69, in which (B) indicates the EDS layered image, which gives information about Area austenitic matrix, area, and the carbide. In Figure 68B, Figure 69B, the presence of sulphur and silicon alloy in the austenitic matrix was observed.

4.2.2.3. E.D.S analysis of HT-3

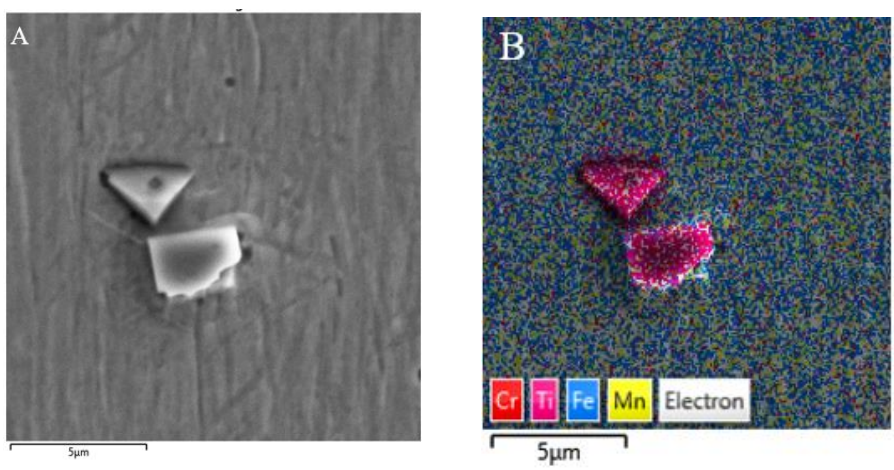

Figure 70 : *(A) SEM image of a carbide found in the top area of the surface material Z. (B) EDS Layered image*

The Energy-dispersive spectroscopy (EDS) analysis of grade (Z) heat-treated under HT3 condition were observed as shown in Figure 70, in which (B) indicates the EDS layered image, which shows us about the austenitic matrix and the carbide. With the presence of titanium as primary carbide. Moreover, for grade Z, there was homogenous dispersion of iron, chromium, and manganese chemical compositions in an austenitic matrix.

4.2.2.4. E.D.S analysis of HT-4

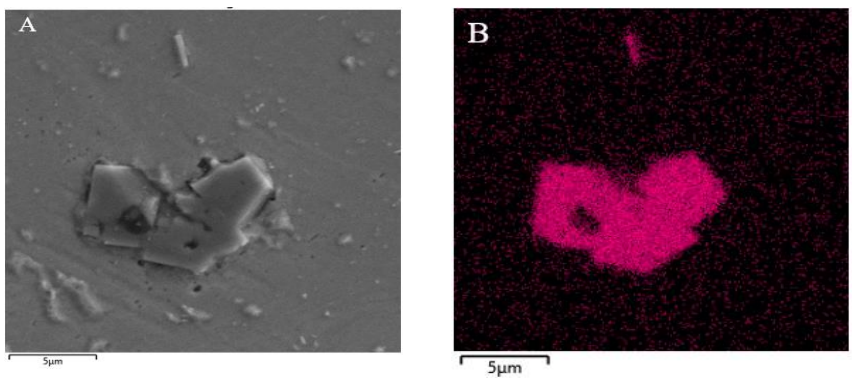

Figure 71: *(A) SEM image of a carbide found in the top area of the surface material X. (B) EDS Layered image*

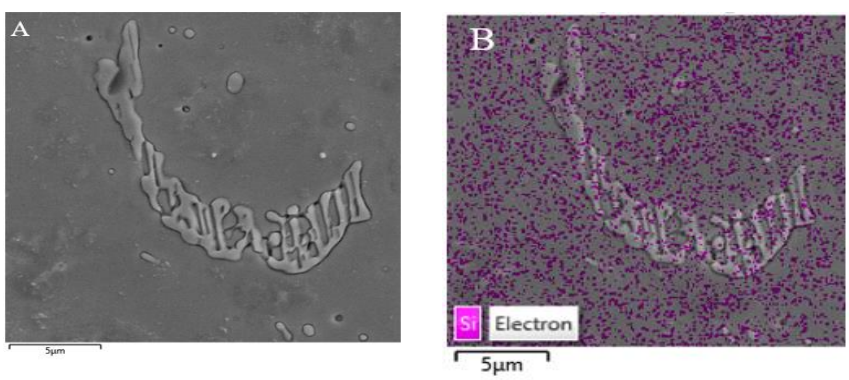

Figure 72 : *(A) SEM image of a carbide found in the top area of the surface material Z (B) EDS Layered image*

In Figure 71, Figure 72, Energy-dispersive spectroscopy (EDS) analysis of grade (X and Z) heat-treated under HT4 condition are shown. Figure (B) indicates the EDS layered images of the carbide. A pleasing heart structure titanium as a primary carbide was observed in Figure 71.

4.2.3. Hardness Test Results

The hardness test was performed on the polished surface of all the samples. All the Hardness measurements were eventually done with a THV-1MDT Automatic Turret Micro Vickers hardness tester. Vickers microhardness testing was done on all the samples with five indentations, which even included on the carbides. We used a 1 kg load with a dwell time of 5 seconds for loading. For this hardness test, all the indentations' mean value is considered the final hardness result.

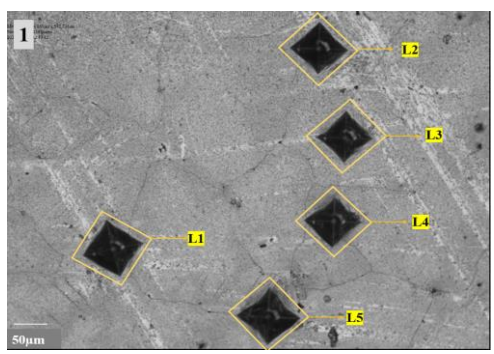

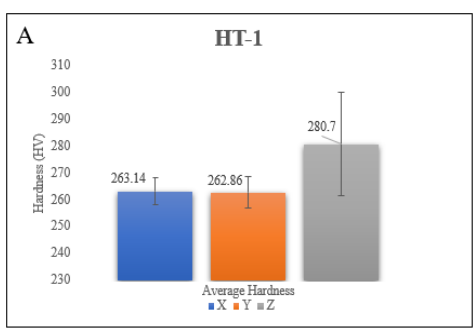

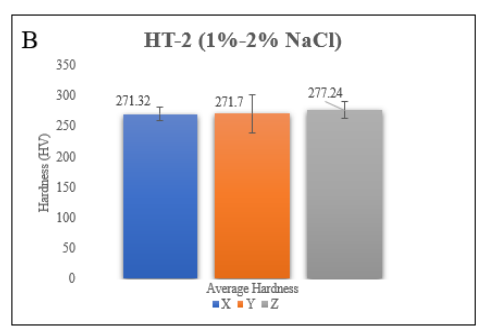

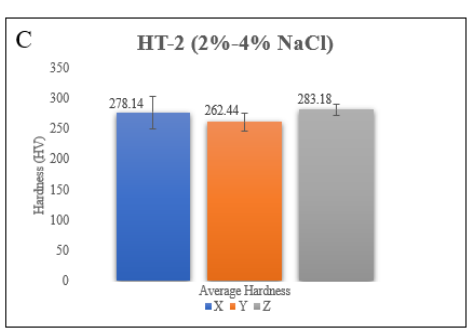

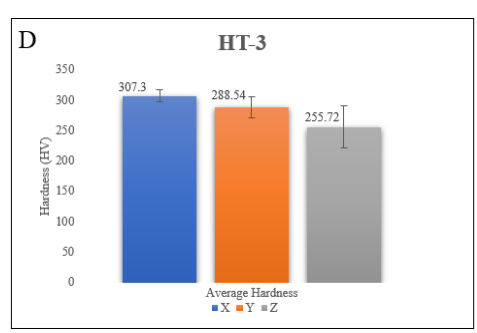

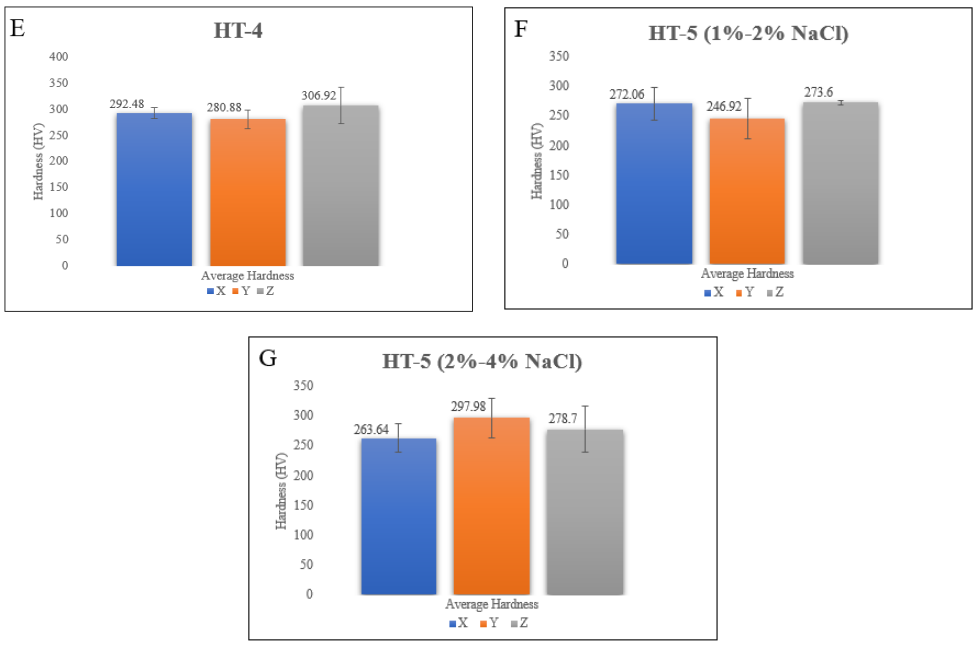

Figure 73 : *(1) Indentation region (L1-L5) on the sample, L1 is on the Carbide (A -G) Average hardness plots for X, Y and Z*

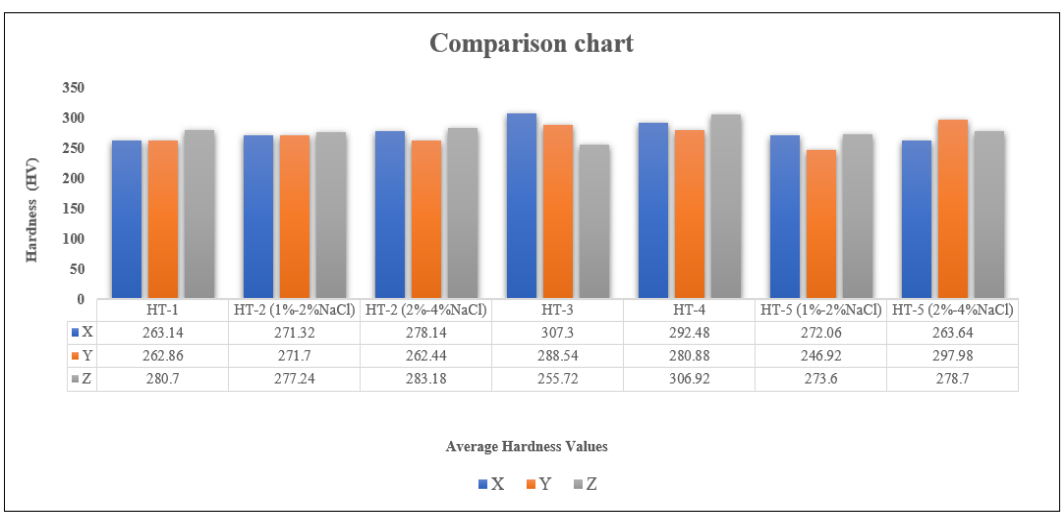

Figure 74 : *A comparison chart of average hardness values with respect to steel grades under different heat treatment cycles*

From Figure 74, We can see that the hardness value for HT-3 grade X has the highest hardness among all, and the rest are in a similar range. This has happened because of the higher %Cr in the material and solubility in the austenite phase. Increased strength and hardness have resulted from the higher amount of solid solution [62]. Additionally, we have also seen the trend in Figure 74; that The values concerning HT-1 and HT4 have been optimal, with grade Z having a slighter increase in the hardness value compared to the grades (X, Y). At the same time, we know that the wear resistance and hardness are directly proportional. Therefore, an increase in hardness is the increase in wear resistance. Therefore, all the heat treatment cycles have been successful as they have slightly higher values than that of the standard samples.

4.3. Discussion

As seen in Figure 34, the microstructure of manganese steel heat treated under HT-1 condition (Table 3) consists of two phases, the austenite phase and carbide phase. Carbides are present because there is an abundance of C and carbide-forming elements like Mn and Fe. Due to the high amount of C and Mn content, the presence of austenitic matrix is observed. Carbides within the matrix, especially $(Fe\ Mn)_3C$ type carbides along or around the grain boundary, spherical or rod-type carbides, and eutectic carbides, are the types of carbides that impact the performance of Hadfield steels. EDS analysis gives elements present in one of the given Hadfield manganese steels. Figure 41, shows the grain boundary carbide precipitation, which is the cause of reduced mechanical properties, which is directly associated with slowing cooling. When there is a presence of carbide, or any other brittle element which are structured unevenly has poor mechanical properties when transformed into austenite. Due to slow heating, internal cracks were avoided.

The experimental Heat treatment (HT-1) consisting of two-step solutionizing and further performing aging gives the fine-grain boundaries for all the three steel grades (X, Y, Z) Figure 24. Steel grade Z showed delicate grain boundaries than X and Y, which means it has a lower amount of carbide present on grain boundaries as well as in an austenitic matrix. A lower

carbide content indicates more carbon is dissolved in the austenitic phase. Two-step heating offers outstanding solubility of carbides as the soaking time is more, longer the holding time at solutionizing, higher the carbides are dissolved, and consequently, there will be more supersaturated austenite. Carbon thus transforms into fine carbide precipitate after staying in this supersaturated austenite for a longer time. A longer holding time with more significant supersaturation is needed for the fine precipitation of carbides. The precipitated, as mentioned, are visually undetectable and produce a very fine dimensional stream. They are visible only at high magnification (50x and 100x) (Figure 36Figure 37). Due to slow heating of 100 °C/hr followed by soaking at 600°C -900°C, it was observed to provide the optimum combination of microstructure and hardness (Figure 56Figure 58) shows the SEM micrographs of the experimented steels, heat-treated cycle HT-1. A minimal number of undissolved carbides was also noticed in samples X, Y, and Z. These carbides are dispersed in the matrix. The presence of these carbides after heat treatment explains that (HT-1) cannot dissolve all the secondary carbides formed during solidification. When the average hardness of sample X, Y, Z samples is compared Figure 73 (D) it is found that the heat-treated Z grade sample has the maximum hardness. Still, the difference between it and the other two grade samples, X and Y, is negligible. This demonstrates that the sample heat-treated under HT-1 condition has optimum hardness and has more acceptable grain boundaries, which are directly proportional to increase impact strength and elasticity [29]. Due to slow heating, internal cracks were avoided.

The experimental Heat treatment-2 samples which shows connected carbides on grain boundaries as well as dispersed carbides in austenitic matrix Figure 38. However, the amount of carbides present is much lesser than as quenched in 2%-4% NaCl solution. The occurrence of fewer carbides in the sample quenched in 1%-2% NaCl solution is a crucial element to emphasize. This is because of the fact that salt has a higher quenching rate compared with pure water. As a result, the sample quenched in salt bath has reacted swiftly through the carbide formation region, leaving less time for C to react with Mn and Fe. The microstructure of grades X, Y, and Z contained carbides and inclusion in the austenitic matrix, as shown in Figure 39, Figure 40. Microstructure in SEM shows the presence of inclusion with carbide;

samples X and Y have more amount of inclusion as compared to Z and are in a spherical shape (Figure 39). When the average hardness of sample X, Y, Z samples are compared (Figure 73(D)), all three samples' value was close enough further, resulting in reaching optimum value.

Heat treatment 2 B (2%-4% NaCl solution) had many flaws when observed after an optical microscope. Carbides were formed at austenite grain boundaries and within the austenite matrix's inner grains. This finding was also seen in other studies [63]. Carbides precipitating and depositing at grain boundaries affected the strength of the material, further decreasing the impact strength and ductility, particularly in heavier parts. Also, continuous carbide precipitation at grain boundaries of the austenite matrix might result in catastrophic failure. Furthermore, the presence of inclusions near austenitic grain can develop cracks. Thus, this heat treatment cycle was excluded from the analysis.

For Heat treatment 3, a dispersed carbide in the grain boundary was obtained. In the Z grade sample, there was a homogenous distribution of carbides in the austenitic matrix compared to a sample of grades X and Y. Intriguingly, cracks were also found in all the samples. Thus, steel grade X has coarser grains, and carbides exist along the grain boundaries. Moreover, the hardness of sample grade X is higher than that of Y and Z (Figure 73 (E)) due to the presence of carbides in the austenitic matrix.

Heat treatment 4, shows the minute number of carbides present in grain boundaries. Samples of grade Y and Z processed by this heat treatment did not appear to have any carbide (Figure 50, Figure 51). When the material is heated to austenitization temperature, the entire structure turns into 100% austenite. Pre-isothermaling at 500℃ - 800℃ gives smaller grain size; further austenitization at 900℃-1100℃ provided more refined grains. The austenite transformation temperature for manganese steel for a concentration of 1%-2% of Carbon (C) begins at 950℃ [47]. When the temperature rises over this temperature, the carbide $(Fe, Mn)_3C$ dissolves into the austenite matrix and forms a solid solution. The quick cooling was carried out to avoid carbide reformation. Step heat treatment methods are an effective and efficient heating process to bring about the formation of 100% austenite structure and produce a more refined grain to increase the impact value of

the manganese steel. The hardness value of sample grade Z is higher than the other two sample grades. This may be reasoned due to the presence of carbide both at the austenite grain boundaries and in the matrix, as seen in the microstructure of the tempered sample (Figure 73(F)).

For Heat treatment 5, a step heating followed by quenching in (1%-2% NaCl) solution shows fine-grain boundaries with unconnected carbides around them. Furthermore, increasing the quenching environment rate and lowering the carbide concentration in the matrix resulted in an increase in soluble carbon content in the austenite phase, further enhancing the hardness [64]. In addition, the hardness of all three steel grades was almost similar. Steel grade Z is higher than steel X, followed by steel Y because of the higher carbon content and chromium content, respectively.

In the case of Steel grade X, it has the least amount of carbon and manganese content when compared to grade Y, and Z. Heat treatment 1 (Figure 34Figure 37), Heat treatment 4 (Figure 48-Figure 50), and heat treatment 5 (Figure 52, Figure 55) give higher results as compared to standard heat treatment. Since more acceptable grain boundaries with fewer secondary carbides were achieved in the microstructure. Also, the hardness of the material was not affected and was in the range of the standard set value given. As this grade contains a little higher %Cr, which stresses carbide formation around the grain boundaries, it is reasonable to have higher hardness than in other steel grades (Figure 73). The results agree with the literature [15]. Therefore, higher solutionizing temperatures (1000°C - 1200°C) are employed since Cr stabilizes iron carbide.

For the given Steel grade Y, which has a moderate amount of carbon and manganese content when compared to steel grade X and Z. Heat treatment 1 (Figure 34, Figure 37), Heat treatment 2(1%-2% NaCl) (Figure 39, Figure 40), and Heat treatment 4 (Figure 48, Figure 50) has optimum result as compared to the heat treatment used by industry. However, there was the presence of inclusions. These heat treatment cycles achieved less carbide in grain boundaries and austenitic matrix for steel grade Y than industrial standard HT cycle. Hardness values of steel grade Y were slightly increased, and Heat treatment 2(1%-2% NaCl) was determined to be the highest (Figure

73b) except in heat treatment cycle 1. The reason is due to the higher content of carbon than X steel grade.

For the steel grade Z, which has a higher amount of carbon and manganese content when compared to steel grade X and Y, Heat treatment 1 (Figure 36Figure 39) Heat treatment 2 (1%-2% NaCl) (Figure 41, Figure 42), Heat treatment 3 (Figure 44) and Heat treatment 4 (Figure 50, Figure 52) offered higher results in the microstructure. Fine-grain boundaries were observed with less carbide content. HT-1 provides strict grain boundaries. Figure 36 and HT-4 offered very little carbide on grain boundaries, almost zero when observed with low magnification. The hardness value for this steel grade was in the range of standard steel and followed high compared to steel X and Y for all heat treatment cycles, except in HT-3. The reason is because of the presence of a higher amount of carbon content in his material. Thus, with finer microstructure and optimum hardness value, Heat treatment-1 and Heat treatment-4 provides promising results. The below table shows obtained results for three different grades (X, Y, Z) when heat treated under five other conditions.

Table 5: *Results achieved when heat treated under five different conditions.*

Heat treatment No	Steel Grade
HT-1	X, Y, Z
HT-2 (1%-2%NaCl)	Y, Z
HT 3	Z
HT-4	X, Y, Z
HT-5	X

After going through the literature review, we can deduce that the Steel grades (X, Y, and Z) show finer grain boundaries when heat treated under conditions mentioned in the Table 5 respectively, that means it has fewer carbides content around the grain boundaries, fewer carbides indicated that the material has an improved impact toughness, this is due to the presence of finer grains which provides more grain boundaries, more the existence of grain boundaries, the tougher it is for dislocations to move, causing an

increase in strength and ductility. As we can observe that experimented with Heat treatment 1 (Figure 37) and Heat treatment 4 (Figure 50) have finer grain boundaries for all three steel grades when compared to other heat treatment cycles, a study from literature says there will be an increase in impact toughness [65]. Thus, impact toughness is correlated with obtained microstructure.

The wear resistance of a material is usually determined by the hardness and number of carbides. From the literature review, the study tells us that the formation of suitably dispersed hard carbides in the austenitic matrix of the steel appears to be a reasonable method to improving the wear resistance of austenitic manganese steels without severely compromising their toughness [66]. Therefore, from table 5, when steel grades (X, Y, and Z) are subjected to respective heat treatment conditions, the dispersion of carbides in the austenitic phase is attained to be homogenous. Also, ideal number of carbides was observed. Moreover, as wear resistance is directly proportional to hardness, from Figure 74, we observe that the hardness of all the steel grades is slightly higher when compared with standard set values.

5. Conclusion

As we know, Hadfield steel is one of the dominant sets of steel families, meant for performing at various conditions, which indeed requires various mechanical properties. Consequently, there is an absolute necessity for the development of heat treatment cycles to balance properties. Toughness and strength, in particular, are often seen as argumentative and are influenced by a variety of parameters, including the composition, types, and nature of carbides and the Heat Treatment parameters. All of these factors were the focal point of our thesis.

Following this examination, we have found that Precipitation hardening or aging, quench hardening, pro-isothermal heating, and the use of Aqueous salt solution have been successful and complement the literature review. But when it comes to rank them according to the microstructural and mechanical properties, from the previous discussion, we have seen that Ageing (HT-1) has been more effective in refining the grain boundaries and has optimal results of the mechanical properties. So this is ideal to be ranked at first place concerning all the three grades and especially to grade Z. Grade Z has been the spotlight of analysis in terms of Optical microscopy, SEM, EDS, and hardness for HT-1, HT-2 (1%-2% NaCl), HT-3 and HT-4, Specially in HT-4 which was to improvise the impact energy. Now coming to the HT-2A(1%-2% NaCl Solution), we could see the optimal results for all three grades with microscopic cracks and shrinkages on it due to inclusions. HT-3 has cracks and inclusions. At the same time, the HT-4 gave us more refined grain boundaries amongst all. Different grade types have varying degrees of hardness for the same Heat Treatment Cycle. Finally, HT-5 has shown unconnected carbides around the grain boundaries.

This generalization is merely based on the Microstructure and the Hardness test (wear-resistance) as they are interconnected. But this could have been more informative with the Wear and impact test results. Despite these challenges, the findings contribute to our understanding of how Hadfield steels act, what kind of changes they go through as they attain their desired states to different temperatures, and how well chemical compositional alterations might affect and influence the Hadfield steel.

6. Future work

A multitude of parameters shapes the material properties of Hadfield steel; however, in this study, the focus has been only on microstructure, hardness, and carbides. Other aspects, such as cooling rate, aging time, and X-RD analysis (to know more about the crystalline phases present in a material), should be investigated to provide a definitive explanation of what causes microstructural variation.

One of the main limiting factors in this project has been the lack of time for testing the wear resistance of the heat-treated samples. Impact testing should also be carried out for the rigorous assessment of the influence of heat treatment cycles on both microstructure and mechanical properties. Also, to shed some light on the assessment regarding the measurement of mechanical properties in terms of heat curves and sizes (hardness and toughness).

If we think the SEM data is contradictory, it may be required to investigate further using Atom Probe Tomography (APT) to precisely characterize the alloy carbides in the Hadfield steel. Subsequently, when it came to the experimental steel grades (X, Y, and Z), the study was complicated by the fact that various parameters, which were altered from Steel X to Steel Z. This depicted attribute a single property change to a single compositional change. Additionally, initial operational and handling costs related to Heat Treatments, quenching methods, and Safety assessment have not been considered for this thesis. Still, they are also the critical parameters for the industrial level and have not been studied in this thesis.

Finally, as we also know, quenching is one of the essential parameters for heat treatment. Our study focused on an aqueous medium quenchant. But there is a wide range of quenchants to choose from, like oil, salt baths, etc. It was planned to use the molten salt bath of both $NaNO_3$ (Sodium Nitrate) and NaCl (Sodium Chloride) for martempering. And could not be performed for safety reasons. Martempering can also be studied to get a carbide-free grain boundary, a better combination of hardness and toughness, better plastic flows, etc.

7. References

[1] Farzam, M. Sabzi and a. Mansour, "Hadfield manganese austenitic steel: a review of manufacturing processes and properties," *Material Research Express,* vol. 6, pp. 1-16, 2019.

[2] D. Havel and P.E, "Austenitic Manganese Steel - A Complete Overview," Columbia Steel Casting Co., Inc., Sepetember 2017.

[3] M. Liang, C. Huang, K. Dolman, X. Tang, J. Yang, Z. Shi and Zhong-Sheng, "A method to calculate the bulk hardness of metal matrix composite using Hadfield steel reinforced with niobium carbide particles as an example," *Mechanics of Materials,* vol. 112, pp. 154-162, 2017.

[4] A. J.O, T. S. and a. A. A. , "On the comparison of microstructure characteristics and mechanical properties of high chromium white iron with the hadfield austenitic manganese steel," *Journal of Minerals and Materials Characterization and Engineering,* vol. 1, pp. 24-28, 2013.

[5] H. Jafarian, M. Sabzi, S. M. Anijdan, A. Eivani and N. Park, "Influence of austenitization temperature on microstructural developments, mechanical properties, fracture mode and wear mechanism of Hadfield high manganese steel.," *Journal of Materials Research and Technology,* vol. 10, no. j.jmrt.2020.12.003., pp. 819-831, 2020.

[6] S. Hosseini, M. B. Limooei, M. H. Zade, E. Askarnia and Z. Asadi, "Optimization of Heat Treatment Due to Austenising Temperature, Time and Quenching," *World Academy of Science, Engineering and Technology International Journal of Materials and Metallurgical Engineering,* vol. 7, no. 7, pp. 582-586, 2013.

[7] S. Alyaz, "EFFECTS OF HEAT TREATMENT AND CHEMICAL COMPOSITION ON MICROSTRUCTURE AND MECHANICAL PROPERTIES OF HADFIELD STEELS," Graduate School of Applied Sciences, The Middle East Technical University, 2003.

[8] D. E. Strohecker, A. G. and &. F. W. , “Deformation Processing of Precipitation-Hardening Stainless Steels. NASA SP-5088,” *Deformation Processing of Precipitation-Hardening Stainless Steels,* p. 255, 1968.

[9] “ ASTM A 128-75a,,” in *Annual Book of ASTM Standards, Part 2,* Philadelphia, PA, ASTM,, 1979, p. 95.

[10] J. I. Erausquin and ., “Reinforcement of Austenitic Manganese Steel with (TiMo) Carbide Particles Previously Synthesized by SHS,” *ISIJ International,* vol. 49, no. 4, pp. 582-586, 2009.

[11] ASTM International, “ASTM A128/A128M-19,” in *Standard Specification for Steel Castings, Austenitic Manganese*, ASTM International, 2019, p. 3.

[12] U. Gürol and a. S. C. Kurnaz, “EFFECT OF CARBON AND MANGANESE CONTENT ON THE MICROSTRUCTURE AND MECHANICAL PROPERTIES OF HIGH MANGANESE AUSTENITIC STEEL,” *Journal of Mining and Metallurgy, Section B Metalurgy,* vol. 2, no. 56, pp. 171-182, 2020.

[13] L. C. Canale, L. A. G. E. T. and L. M. , “HARDENABILITY OF STEEL,” [Online]. Available: https://edisciplinas.usp.br/pluginfile.php/5789230/mod_resource/content/1/Hardenability%20Lauralice.pdf. [Accessed 20 02 2021].

[14] M. Maalekian, “The Effects of Alloying Elements on Steels (I),” *Institut für Werkstoffkunde, Schweißtechnik und Spanlose Formgebungsverfahren,* p. 36, 2007.

[15] E.-M. I., R. Abdel-karim and A.Naguib, “Evalution of effect of chromium on wear performance of high managanese steel,” Department of metallurgy, 2000.

[16] ASM International, “Alloy Phase Diagrams,” in *ASM Handbook, Volume 3,* H. Baker, Ed., ASM International, 1992, pp. 1.1-1.29 .

[17] A. Caesar, “Wikimedia Commons,” Wikimedia Commons, 27 02 2019. [Online]. Available: https://commons.wikimedia.org/wiki/File:Iron_carbon_phase_diagram.svg. [Accessed 10 02 2021].

[18] M. H-Rasheed, “Engineering Metallurgy,” University of Babylon, College of Engineering, Babylon, Iraq.

[19] Hasse, Fredriksson, Stefanescu and D. M., “Principles of Thermal Analysis,” in *ASM HAndbook, Cast Iron Science and Technology*, ASM International, 2017.

[20] K. H. Prabudeva, Handbook of Heat-treatment of Steels, New Delhi: TATA McGRAW-HILL PUBLISHING COMPANY LIMITED, 1988.

[21] A. L. Kumar, D. and a. D. S.K.Badjena, “University of Cambridge,” 2012. [Online]. Available: https://www.phase-trans.msm.cam.ac.uk/2012/Manna/Part2.pdf. [Accessed 16 02 2021].

[22] B. Harshad and H. Robert, Steels: Microstructure and properties (Fourth Edition), Amsterdam: Butterworth-Heinemann ISBN 9780081002704,, 2017.

[23] C. Smith, “A history of martensite: Early ideas on the structure of steel,” in *Martensite*, Materials Park, OH, ASM International, 1992, pp. 21-39.

[24] Z. Hou, “An experimental and theoretical study of precipitation during tempering of martensite in Fe-C-Cr alloys,” Department of Materials Science and Engineering, School of Industrial Engineering and Management, Royal Institute of Technology, Stockholm, Sweden, 2018.

[25] G. Sil’man, “Phase Diagram of Alloys of the Fe - C - Mn System and Some Structural Effects in this System. Part 1. Interphase Distribution of Manganese,” *Met Sci Heat Treat,* vol. 2, no. 47, p. 2005, 48-52.

[26] A. Rabinkin, “"Iron-Manganese (Fe-Mn) Phase Diagram",” Calphad, 2011. [Online]. Available: https://en.wikiversity.org/wiki/File:Fe-Mn_Phase_Diagram.gif. [Accessed 10 02 2021].

[27] S. Lintzen, J. v. A. B. H. and R. D. , “The Fe–Mn enthalpy phase diagram from first principles,” *Journal of Alloys and Compounds,* vol. 577, pp. 370-375, 2013.

[28] C. Study, “Chapter 10,” in *Introduction to Materials Science for Engineers*.

[29] B. Bandanadjaja and E. Hidayat, “The effect of two-step solution heat treatment on the impact properties of Hadfield austenitic manganese steel,” *Journal of Physics: Conference Series 1450,* no. doi:10.1088/1742-6596/1450/1/012125, 2020.

[30] B. S.W., B. Nyembe and K. Lentsoana, “Common Causes of Premature Failure of Hadfield Steel Crushers and Hammers Used in the Mining Industry,” *INTERNATIONAL JOURNAL of ENGINEERING TECHNOLOGIES-IJET,* vol. 3, no. 2, pp. 83-90, 2017.

[31] D. N.G. and L. V.A., “HEAT TREATMENT OF PARTS AND CASTINGS FROM HIGH-MANGANESE STEEL OF TYPE 110G13L AND ITS SPECIAL FEATURES,” *Met Sci Heat Treat ,* vol. 58, p. 559–561, 2017.

[32] S. Dean, L. & Canale, X. & Luo, X. & Yao and ., “Quenchant Characterization by Cooling Curve Analysis,” *Journal of Astm International,* vol. 6(2), no. 10.1520/JAI101981., p. 44, (2009).

[33] S. MacKenzie, “Overview of the Mechanisms of Failure in Heat Treated Steel Components,” *ASM Internationa,* p. 45, 2008.

[34] R. S. Molla, “A study on Manufacturing of Deformed Bar (G 60-400W) at Elite Iron and Steel Industries.,” 10.13140/RG.2.2.24320.33289., 2018.

[35] R. Morton, “MARQUENCHING AND MARQUENCHING OILS,” *Industrial Lubrication and Tribology,* vol. Vol. 20 , no. No. 9, https://doi.org/10.1108/eb052873, pp. 301-309, 1968.

[36] P. SEDLAK, H. SEINER, M. FROST, L. HELLER, O. TYC, L. KADERAVEK and P. SITTNER, “COUPLED TRANSFORMATION AND PLASTICITY IN NITI,” [Online]. Available: http://www.lem3.univ-lorraine.fr/ESOMAT2018/Abstracts/Session9/222.pdf. [Accessed 15 02 2021].

[37] J. V. ,. G. E. T. Lauralice de C.F. Canale, “Martempering of Steels,” in *Steel Heat Treating Fundamentals and Processes, Vol 4A*, ASM International, 2013, p. 362–381.

[38] H. Luís, Z. Pizetta, V. A. Oliveira, T. G. E. and C. L. C.F., “Quenching power of aqueous salt solution,” *International Journal of Heat and Mass Transfer,* vol. 140, no. https://doi.org/10.1016/j.ijheatmasstransfer.2019.06.036, pp. 807-818, 2019.

[39] G. Krauss, “Principles of heat treatment of steel,” *American Society for Metals,* p. 291, 1980.

[40] G. Ramesh and K. Narayan Prabhu, “Spatial Dependence of Heat Flux Transients and Wetting Behavior During Immersion Quenching of Inconel 600 Probe in Brine and Polymer Media.,” *METALLURGICAL AND MATERIALS TRANSACTIONS B,* vol. 45B, no. https://doi.org/10.1007/s11663-014-0038-7, pp. 1355-1369, 2014.

[41] M. F. Beck and P. Archambault, “Effect of workpiece surface properties on cooling behavior,” *Quenching Theory and Technology,* pp. 289 - 313.

[42] J. A. Venables, “Deformation twinning in face-centred cubic metals,” *The Philosophical Magazine: A Journal of Theoretical Experimental and Applied Physics* , vol. 6, no. https://doi.org/10.1080/14786436108235892, pp. 379-396 , 1961.

[43] K. I., S. H., C. Yury, H. Maie and I. Kireeva, “Extrinsic stacking faults and twinning in Hadfield manganese steel single crystals,” *Scripta Materialia - SCRIPTA MATER,* vol. 44, no. 10.1016/S1359-6462(00)00600-X., pp. 337-343, 2001.

[44] C. Mahlami and X. Pan, “An Overview on high manganese steel casting,” *71st World Foundry Congress: Advanced Sustainable Foundry,* 2014.

[45] J. Tasker and M. Amuda, “Austenitic Steels: Non-Stainless,” *Reference Module in Materials Science and Materials Engineering,* no. 10.1016/B978-0-12-803581-8.09206-7, 2017.

[46] C. Xiaohui, L. Jia, C. Xu, W. Huaming and H. Zheng, “Effect of heat treatment on microstructure, mechanical and corrosion properties of austenitic stainless steel 316 L using arc additive manufacturing,” *Materials Science and Engineering A.175,* no. 10.1016/j.msea.2017.10.002, 2017.

[47] C.-R. E and e. al, “Effect of Carbide Precipitation on the Structure and Hardness in the Heat-Affected Zone of Hadfield Steel After Post-Cooling Treatments,” *Materials and Manufacturing Processes,* vol. 23, no. 10.1080/10426910701524352, pp. 14-20, 2007.

[48] El-Rakayby and M. B. A.M., “On the microstructure and mechanical properties of high-speed steels.,” *JOURNAL OF MATERIALS SCIENCE,* vol. 23, no. https://doi.org/10.1007/BF00551928, pp. 4340-4344, 1988.

[49] S. Kuyucak, R. Zavadil and V. Gertsman, “Heat-treatment Processing of Austenitic Manganese Steels,” Istanbul, Turkey, 2004.

[50] R. Z. V. G. Selçuk Kuyucak, “Heat-treatment Processing of Austenitic Manganese Steels”.

[51] H. Jeongho, K. d. S. Alisson, P. D, R. Dierk, L. Sang-Min, L. Young-Kook, Lee, Sang-In, Hwang and Byoungchul, “The effects of prior austenite grain boundaries and microstructural morphology on the

impact toughness of intercritically annealed medium Mn steel," *cta Materialia.,* vol. 122, pp. 199-206, 2016.

[52] S. Hosseini, M. B. Limooei, M. H. Zad, E. A. and Z. Asadi, "Optimization of Heat Treatment Due to Austenising Temperature, Time and Quenching Solution in Hadfield Steels," *International Journal of Materials and Metallurgical Engineering,* vol. 7, no. https://publications.waset.org/pdf/16553, pp. 582-585, 2013.

[53] Limooei, S. Hosseini and M. Bagher, "Optimization of Heat Treatment to Obtain Desired Mechanical Properties of High Carbon Hadfield Steels," *World Applied Sciences Journal. ,* vol. 15, 2011.

[54] O. Zambrano, J. Valdés, Y. Aguilar, J. Coronado, S. Rodríguez and R. E. Logé, "Hot deformation of a Fe-Mn-Al-C steel susceptible of κ-carbide," *Materials Science and Engineering: A,* vol. 689, no. https://doi.org/10.1016/j.msea.2017.02.06, pp. 269-285, 2017.

[55] K. Panchal, "Life Improvement of Hadfield manganese steel castings," *International Journal of Scientific Development and Research ,* vol. 1, no. 5, pp. 817-827, 2016.

[56] W. B.A and P. P.C, "A Review of Steel Processing Considerations for Oxide Cleanliness," *Metall Mater Trans B,* vol. 51, no. https://doi.org/10.1007/s11663-020-01949-y, p. 2437–2452, 2020.

[57] F. Pablo and S. Leandro, "Effect of titanium and nitrogen inoculation on the microstructure, mechanical properties and abrasive wear resistance of Hadfield Steels.," *REM - International Engineering Journal,* vol. 73, no. 10.1590/0370-44672019, pp. 77-83, 2020.

[58] K. Panchal, "Life Improvement of Hadfield manganese steel castings," *International Journal of Scientific Development and Research (IJSDR),* vol. 1, no. 5, pp. 817-825, 2016.

[59] S. A. Ibitoye, J. O. Olawale and M. D. Shittu, "MECHANICAL PROPERTIES OF QUENCH-HARDENED, MARTEMPERED AND

TEMPERED ASTM A 128 GRADE B-4 STEEL," *Journal of Science and Technology,* vol. 29, no. 2, pp. 107-112, 2009.

[60] Struers, "Struers," Struers, [Online]. Available: https://www.struers.com/en/Products/Grinding-and-Polishing/Grinding-and-polishing-equipment/Tegramin#. [Accessed 10 05 2021].

[61] "Tescan Korea," Tescan, [Online]. Available: http://www.tescan.co.kr/product/em/em02. [Accessed 11 05 2021].

[62] K. D. Ashok Kumar Srivastava, " In-situ Synthesis and Characterization of TiC-reinforced Hadfield Manganese Austenitic Steel Matrix Composite," *ISIJ International,* vol. 49, no. 9, pp. 1372-1377, 2009.

[63] M. Azadi, A. M. Pazuki and M. J. Olya, "The Effect of New Double Solution Heat Treatment on the High Manganese Hadfield Steel Properties," *Metallography, Microstructure, and Analysis,* no. 5, 2018.

[64] C. Zhang, Y. K. B. H. and .. e. al, "Corrosion-resistant carbide-reinforced martensitic steel by Cu modification.," *npj Materials Degradation,* vol. 3, no. 30 https://doi.org/10.1038/s41529-019-0092-3, 2019.

[65] M. Gedeon, "Grain Size and Material Strength," *Technical Tidbits,* no. 15, p. 2, 2010.

[66] J. C. ,. T. R.-O. ,. A. H. ,. L. B. ,. A. d. R. &. M. E. R. E. Curiel-Reyna, "Effect of Carbide Precipitation on the Structure and Hardness in the Heat-Affected Zone of Hadfield Steel After Post-Cooling Treatments," *Materials and Manufacturing Processes,* vol. 23, no. 1, pp. 14-20, 2007.

[67] A. K. S. Æ. K. Das, "Microstructural characterization of Hadfield austenitic manganese steel".

[68] M. Banerjee, “Fundamentals of Heat Treating Metals and Alloys,” in *Comprehensive Materials Finishing, Volume 2*, Jaipur, India, Elsevier Inc., 2017, p. 49.

[69] F. Fracasso, “INFLUENCE OF QUENCH RATE ON THEHARDNESS OBTAINED AFTER ARTIFICIAL AGEING OF AN Al-Si-Mg ALLOY,” Jönköping Institute of Technology, Jönköping, Sweden, 2010.

[70] S. Balogun, D. E. Esezobor and J. O. Agunsoye, “Effect of Melting Temperature on the Wear Characteristics of Austenitic Manganese Steel,” *Journal of Minerals and Materials Characterization and Engineering*, vol. 7, no. 3, pp. 277-289, 2008.

[71] J. JIN, R. GAO, H. PENG, H. GUO, S. GONG and B. CHEN, “Rapid Solidification Microstructure and Carbide Precipitation Behavior in Electron Beam Melted High-Speed Steel,” *METALLURGICAL AND MATERIALS TRANSACTIONS A*, vol. 51A, pp. 2411-2429, 2020.